

Review

# Effect of Nanoparticle Interaction on Structural, Conducting and Sensing Properties of Mixed Metal Oxides

Leonid I. Trakhtenberg<sup>1,2</sup>, Maria I. Ikim<sup>1</sup>, Olusegun J. Ilegbusi<sup>3,\*</sup>, Vladimir F. Gromov<sup>1</sup>  
and Genrikh N. Gerasimov<sup>1</sup>

<sup>1</sup> N.N. Semenov Federal Research Center for Chemical Physics, Russian Academy of Sciences, 119991 Moscow, Russia

<sup>2</sup> Chemical Faculty, Lomonosov Moscow State University, 119991 Moscow, Russia

<sup>3</sup> Department of Mechanical and Aerospace Engineering, University of Central Florida, Orlando, FL 32816, USA

\* Correspondence: olusegun.ilegbusi@ucf.edu

**Abstract:** This review analyzes the studies published, mainly in the last 10–15 years, on the synthesis, structure, and sensor properties of semiconductor nanocomposites. Particular attention is paid to the interaction between nanoparticles of the sensitive layer, and its effect on the structure, sensitivity, and selectivity of semiconductor sensor systems. Various mechanisms of interaction between nanoparticles in metal oxide composites are considered, including the incorporation of metal ions of one component into the structure of another, heterocontacts between different nanoparticles, and core-shell systems, as well as their influence on the characteristics of gas sensors. The experimental data and studies on the modeling of charge distribution in semiconductor nanoparticles, which determine the conductivity and sensor effect in one- and two-component systems, are also discussed. It is shown that the model which considers the interactions of nanoparticles best describes the experimental results. Some mechanisms of detection selectivity are considered in the conclusion.

**Keywords:** mixed metal oxide sensor; nanoparticle interaction; morphology; nanoparticle structure; sensitivity; selectivity



**Citation:** Trakhtenberg, L.I.; Ikim, M.I.; Ilegbusi, O.J.; Gromov, V.F.; Gerasimov, G.N. Effect of Nanoparticle Interaction on Structural, Conducting and Sensing Properties of Mixed Metal Oxides. *Chemosensors* **2023**, *11*, 320. <https://doi.org/10.3390/chemosensors11060320>

Academic Editors: Elisabetta Comini and Ana Rovisco

Received: 24 April 2023

Revised: 21 May 2023

Accepted: 23 May 2023

Published: 26 May 2023



**Copyright:** © 2023 by the authors. Licensee MDPI, Basel, Switzerland. This article is an open access article distributed under the terms and conditions of the Creative Commons Attribution (CC BY) license (<https://creativecommons.org/licenses/by/4.0/>).

## 1. Introduction

Sensors based on semiconductor metal oxides are currently widely used to detect various gases in the environment. The principles for production of highly efficient sensors, based on metal oxides, for the detection of various substances have been investigated for more than four decades (see, for example, reviews [1–5]). In this review, we consider studies elucidating the influence of the composition, structure, and chemical properties of semiconductor composites, on the sensor characteristics, undertaken mainly in the last 10–15 years. Particular attention is paid to the interaction between the components of nanostructured composites and its effect on the chemical processes that determine the operational properties of metal oxide sensors. All the studies cited below have used composites prepared by different methods, including the mixing of ready-made nanopowders, various impregnation methods, hydro- and solvothermal treatment, the sol-gel technique, the electrospinning method, and others. The techniques used for the preparation of different composites in the literature and associated references are summarized in two tables in a subsequent section.

The operation of metal oxide sensors is based on the change in their conductivity, under the influence of the analyzed gases. Depending on the oxygen content in the environment, this process is described by two different models. The ion-sorption model describes the sensor process at a high oxygen concentration. The chemisorbed oxygen molecules present in the sensitive layer of the particle capture electrons from the conduction band of the metal oxide, creating oxygen anion centers, such as  $O^-$ ,  $O_2^-$ , and  $O^{2-}$  on the surface. As a result, a negatively charged layer is formed on the surface of the nanoparticles, and the

near-surface region is depleted of conduction electrons (the depletion region), due to their escape to the surface from the near-surface layer [6].

The resistance of the sensor depends on the parameters of the barrier that the electrons overcome during the transition between particles, and the concentration of electrons in the layers near the surface of the particles. The distribution of electrons in a nanoparticle is determined by the equilibrium conditions (see Section 3). Correspondingly to the change in the concentration of electrons in the layers near the surface of the particles, the sensor resistance increases.

The interaction of the molecules of the analyzed gas, adsorbed on the surface of metal oxide nanoparticles with the active oxygen centers, results in the release of trapped electrons, which subsequently return to the conduction band of the semiconductor. There occurs an increase in the conductivity of electronic (*n*) semiconductors and a decrease for hole (*p*) semiconductors.

At low oxygen concentrations, for example, to detect impurities of reducing gases in an inert gas, the sensor process proceeds in accordance with the vacancy model [7,8]. In this case, the reducing gas reacts with the oxygen ions of the  $O^{2-}$  lattice of the metal oxide on the surface of the sensitive layer nanoparticles, to form oxygen vacancies containing weakly bound electrons, which also increases the conductivity of the sensor [8]. This review considers the processes occurring in air ambience and therefore, the most common ion-sorption model is used.

The type of oxygen ions adsorbed on the surface of a semiconductor metal oxide depends on temperature (see Figure 1). At temperatures in the range of 200–400 °C, at which metal oxide sensors mainly “work” for the detection of reducing gases, oxygen anions ( $O^-$ ) are the active centers [8–10].

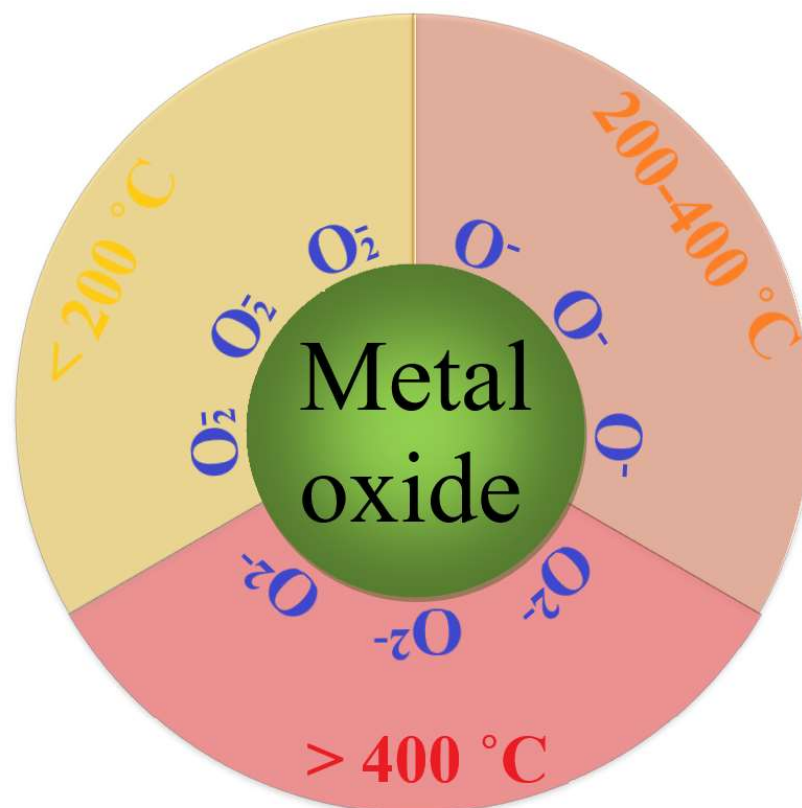


**Figure 1.** Schematic representation of the priority formation of active oxygen species on the surface of metal oxide nanoparticles at different temperatures.

As for the  $O^{2-}$  ions, there are no convincing experimental data on the state and behavior of these particles on the metal oxide surface, and the calculations in some previous

studies [11,12] give contradictory results. In addition, these calculations do not consider surface oxygen vacancies, which play an important role in the sensor process. All of the above support the sensor response model involving the radical ion  $O^-$ .

A generally accepted approach to improving the sensitivity, rate, and selectivity of the sensors is to use composite systems that combine metal oxides with different electronic characteristics and chemical properties (see, for example, [13–20]). Until recently, only systems containing small additives (no more than 5–10%) of modifying oxides were considered in the study of sensor characteristics of metal oxide composites. A detailed study of the behavior of composites containing measurable amounts of different oxides began with the studies in Refs [20–22]. In the last 5–6 years, studies by other authors have appeared, that considered sensor systems consisting of mixtures of oxides over a wide range of compositions (see, for example, [23,24]).

The sensor properties of metal oxide composites are determined by the electronic structure of the nanoparticles, which, in turn, is affected by the interaction between the components of the composite. It is this interaction that determines the sensor activity of metal oxide nanocomposite sensors.

Depending on the relative content of metal oxides, it is reasonable to classify the two-component systems into single-phase and two-phase systems. A single-phase composite is a solid solution in which an ion of the doping oxide enters the lattice of nanocrystals of another oxide. Such solutions are formed only in the range of doping oxide concentrations not exceeding 10%. The difference in the sizes and charges of the ions forming the lattice produces additional deformations and defects in the lattice. This stimulates the adsorption of oxygen and detected gases on the surface of nanocrystals, which increases the sensor effect.

Binary two-phase systems, formed at comparable concentrations of oxides, consist of a solution of a small addition of one oxide (up to 10%) in the lattice of another oxide, without nanocrystal of the first component in the system. The influence of the interaction of components on the sensitivity of the sensor system is due to the contact between nanocrystals of different phases.

An analysis of the available literature shows that the sensor effect of nanostructured metal oxide systems is determined mainly by two factors [25,26]. The first is the chemisorption of the detected gas and oxygen on the surface of sensor particles, and the subsequent interaction of the chemisorbed gas with active oxygen centers. The second factor is the change in the electronic structure of metal oxides during the sensor reaction, which affects the conductivity of the sensitive layer. It is important to note that in a system consisting of metal oxides with different electronic and physicochemical properties, both of the above factors depend on the interaction between these components. This interaction largely determines the behavior of metal oxide nanocomposite sensors and makes it possible to purposefully change their performance characteristics.

Since the metal oxides used in sensors are ionic compounds, their contact in mixed oxide composites can lead to the transition of metal ions of one component into the nanoparticles of another (doping of nanoparticles). This causes the transfer of electrons between particles, their mutual charging, and changes in the structure of the nanoparticles [27,28]. The introduction of small concentrations (up to 5–7%) of metal ions with a higher charge into the metal oxide results in the appearance of an additional positive charge.

Compensation of this charge occurs due to a decrease in the concentration of positively charged oxygen vacancies and an increase in the concentration of conduction electrons. Thus, when  $In_2O_3$  is doped with tin oxide,  $In^{+3}$  ions are replaced by  $Sn^{+4}$  ions, which are accompanied by an increase in conductivity and a decrease in the sensor response to hydrogen [19]. Replacing lattice ions with lower valence ions creates localized negative charges on metal ions embedded in the lattice. In this case, the concentration of positively charged oxygen vacancies in the lattice increases [29], leading to a decrease in the concentration of conduction electrons in the metal oxide.

An important role in the sensor process is also played by the transfer (spillover) of chemisorbed molecules and products of their reactions with metal oxides between the contacting nanoparticles. Thus, a noticeable sensor effect in a system of SnO<sub>2</sub> nanofibers, coated with a layer of catalytically active Pd nanoparticles, is explained by the spillover of oxygen atoms formed on the surface of Pd nanoparticles, upon dissociation of O<sub>2</sub> [30]. Oxygen atoms transfer to SnO<sub>2</sub> nanofibers, capturing conduction electrons from them, and, as a result, are converted into O<sup>-</sup> radical anions.

The sensor process proceeds according to a similar scheme in a system containing comparable concentrations of ZnO and In<sub>2</sub>O<sub>3</sub> [22]. An increase in the sensor effect upon the addition of ZnO occurs because of the spillover of O<sup>-</sup> radical anions formed during the dissociation of oxygen, on catalytically active ZnO, into tin oxide nanoparticles. These O<sup>-</sup> radical anions determine the conductivity of the composite.

The theory of the sensor effect in single-component systems, allowing for the distribution of conductive electrons, was developed in previous studies [14,31–35]. A comparison is made in these studies with experimental literature data, and the approaches of other authors to the description of the sensor process are discussed. The theoretical description of the sensor effect is largely based on the distribution of electrons in semiconductor nanoparticles [31,36,37]. In the case of nanoparticles with high electron content in the conduction band, the important role of the negatively charged layer is considered. Various mechanisms of interaction between nanoparticles are also considered, and the distribution of electrons and the sensor effect in two-component systems is described [37].

## 2. Mechanisms of Sensitivity of Semiconductor Metal Oxide Sensors in the Detection of Reducing Gases

The sensor effect, which characterizes the sensitivity of the sensor, is mainly determined by three factors: the specific surface area of the sensitive nanostructured layer; the adsorption of oxygen and analyzed compounds on the surface of nanoparticles; and the reactivity of adsorbed compounds with respect to active oxygen centers [2].

The sensitivity of semiconductor metal oxide sensors can be significantly increased by using nanostructured sensitive layers based on two-component materials, consisting of metal oxides with different electronic characteristics and chemical properties (see, for example, [13–16]). The mechanisms for the increase in sensitivity depend on the interaction between the metal oxide components, which is affected by their phase state. With this in mind, we will classify sensor systems into *single-phase* and *two-phase* types.

As noted above, a single-phase, two-component system is a solid solution in which metal ions of one component enter the lattice of nanocrystals of another component. The presence in the lattice, of contacting metal ions of different sizes and charges, contributes to the formation of additional deformations and defects in the crystal (in particular, oxygen vacancies), which stimulate the adsorption of oxygen and analyzed gases on the surface of nanocrystals and increase the sensor effect.

However, metastable solid solutions in a two-component metal oxide system are formed only in the region of low doping oxide concentrations, which depend on the size and valence of metal ions, and do not exceed 10%. At higher concentrations, segregation of solid solutions occurs when the particles of the segregated material coexist with the particles of the solid solution [14,19,38].

In binary two-phase systems, the influence of the interaction of components on the sensitivity of the sensor system is due to contacts between nanocrystals of different phases. The transfer of electrons between nanocrystals with different work functions, during the contact of oxides, leads to mutual charging of the nanocrystals [27], which, in turn, affects the adsorption of molecules, especially dipole types.

Of particular interest are contacts between catalytically active metal oxides and electron-rich nanoparticles that form the conduction paths of a sensor system (see, for example, [14,19,39]). In this case, the increase in sensitivity is due to the transition into

conducting nanocrystals of atomic and molecular particles, arising from the dissociation of oxygen molecules and the adsorption of the analyzed gas.

### 2.1. Mechanisms of Increasing the Sensitivity of Two-Component, Single-Phase Metal Oxides

Various processes occur in the sensitive layer of two-component, single-phase metal oxides that affect their properties. In the following sections, we consider the effects associated with the doping of nanoparticles of one component with the molecules or atoms of another. These effects include the change in the particle lattice during doping, the role of doping in the adsorption of oxygen and detected gases, and the influence of the nature of doping ions.

#### 2.1.1. Change in the Lattice of Particles during Doping—Dependence of the Interaction of Doping Ions with Ions of Main Lattice on Their Valence

The formation of binary metal oxide systems, by coprecipitation of components from solutions containing a mixture of salts or organometallic precursors or by impregnation of crystals of one metal oxide with another metal, can be accompanied by the incorporation of one of the components into the crystal structure of the second oxide, i.e., doping [13,16,40]. In this case, the metal ions of the base oxide are replaced by doping ions. There are two types of doping, namely isovalent doping, in which the valences of the main ions that make up the crystal lattice and the doping ions are the same, and heterovalent doping, when the valences of the metal ions are different.

The change in the structure and properties during isovalent doping is due to the deformation of bonds in the main crystal when doping ions are introduced into its lattice, the size of which differs from the size of the main ions. The energy of ionic bonds ( $E_{MO}$ ) in the metal oxide crystal depends on the surface charge density of the cation in the lattice and increases with decreasing cation size.

The influence of lattice deformations on the concentration of oxygen vacancies depends on the method of formation of a two-component system. A typical example is  $In_2O_3$  nanocrystals doped with aluminum oxide. During the formation of  $Al_2O_3-In_2O_3$  nanocrystals from a mixed solution of indium and aluminum salts by electrospinning, the  $In^{+3}$  ions (radius 0.80 Å) are partially replaced by the smaller  $Al^{+3}$  ions (radius 0.54 Å). This leads to the contraction of the lattice of  $In_2O_3$  nanocrystals and their rearrangement into a stronger rhombohedral phase, which is accompanied by an increase in  $E_{MO}$  and a decrease in the concentration of oxygen vacancies [41].

A similar result was obtained for  $SnO_2$  nanocrystals synthesized by electrospinning ( $Sn^{+4}$  radius 0.71 Å) and doped with  $Ti^{+4}$  ions (radius 0.64 Å) [42]. At the same time,  $Al_2O_3-In_2O_3$  nanocrystals formed by the hydrothermal method retain the weaker cubic structure of  $In_2O_3$  crystals. Lattice compression upon the doping of crystals with aluminum ions leads to the formation of defects and an increase in the concentration of oxygen vacancies [43]. These vacancies form centers of oxygen chemisorption, which increase the sensor effect in the detection of reducing compounds [43,44].

An increase in the concentration of oxygen vacancies and the associated increase in the sensor effect are more pronounced because of lattice expansion upon the isovalent doping of metal oxide nanocrystals with metal ions of larger size than the main lattice ions. This is clearly seen in the example of  $In_2O_3$  nanocrystals with  $In^{3+}$  ions (radius 0.80 Å) doped with  $La^{3+}$  ions (radius 1.03 Å) [45,46], which is explained by the weakening of bonds in the  $In_2O_3$  lattice under the influence of  $La^{3+}$  ions.

The most significant effect on the sensitivity of two-component, single-phase metal oxides is provided by heterovalent doping. Due to the difference in the valence of metal ions, not only local deformations but also new local charges arise in the lattice of a nanocrystal. The change in the sensor properties of the metal oxide during doping depends on the ratio of the charges of the doping ions to the main ions of the crystal lattice, which determines the conductivity.

The introduction of up to 5–7% of metal ions with a larger charge into the basic oxide lattice produces an additional positive charge in the system. The concentration of positively charged oxygen vacancies decreases and the concentration of conduction electrons increases. As a result, when  $\text{In}_2\text{O}_3$  is doped with  $\text{SnO}_2$  and  $\text{In}^{3+}$  ions are replaced by  $\text{Sn}^{4+}$  ions, an increase in conductivity and a decrease in the sensor response to hydrogen are observed [19,40].

When lattice ions are replaced by ions with a lower valence, localized negative charges appear on metal ions built into the lattice, the concentration of positively charged oxygen vacancies increases [29], and the concentration of conduction electrons decreases. Such a process is considered in the example of the formation of the  $\text{SnO}_2$ - $\text{In}_2\text{O}_3$  composite [29,40]. Since the size of  $\text{In}^{3+}$  is larger than that of  $\text{Sn}^{4+}$ , the substitution of  $\text{In}^{3+}$  for  $\text{Sn}^{4+}$  results in an increase in interplanar distances in the  $\text{SnO}_2$  lattice and an increase in the response to hydrogen [40,47].

When lattice ions are replaced by doping ions, in contrast to their incorporation into the intercrystallite space, the emerging vacancies can form complexes with these ions. Such complexes were characterized for  $\text{In}_2\text{O}_3$  nanocrystals doped with  $\text{Mn}^{+2}$  and  $\text{Co}^{+2}$  ions [48]. The vacancies formed when these ions are included in the  $\text{In}_2\text{O}_3$  lattice, and enter the first coordination sphere of oxygen anions surrounding the doping ion [49].

Many metal ions form specific bonds with organic molecules. Such complexes, in which the centers of oxygen chemisorption (oxygen vacancies) are associated with the centers of adsorption of the detected gas on embedded metal ions, create especially favorable conditions for the sensor process. Thus, the impregnation of nanocrystalline  $\text{In}_2\text{O}_3$  by divalent cobalt, which is accompanied by the incorporation of  $\text{Co}^{+2}$  ions into the  $\text{In}_2\text{O}_3$  lattice, produces a material with an exceptionally high response to CO (Figure 2) [50]. Impregnation of  $\text{In}_2\text{O}_3$  nanoparticles by other metals also increases the sensor effect, but much less so than in the case of  $\text{Co}^{+2}$  ion incorporation.

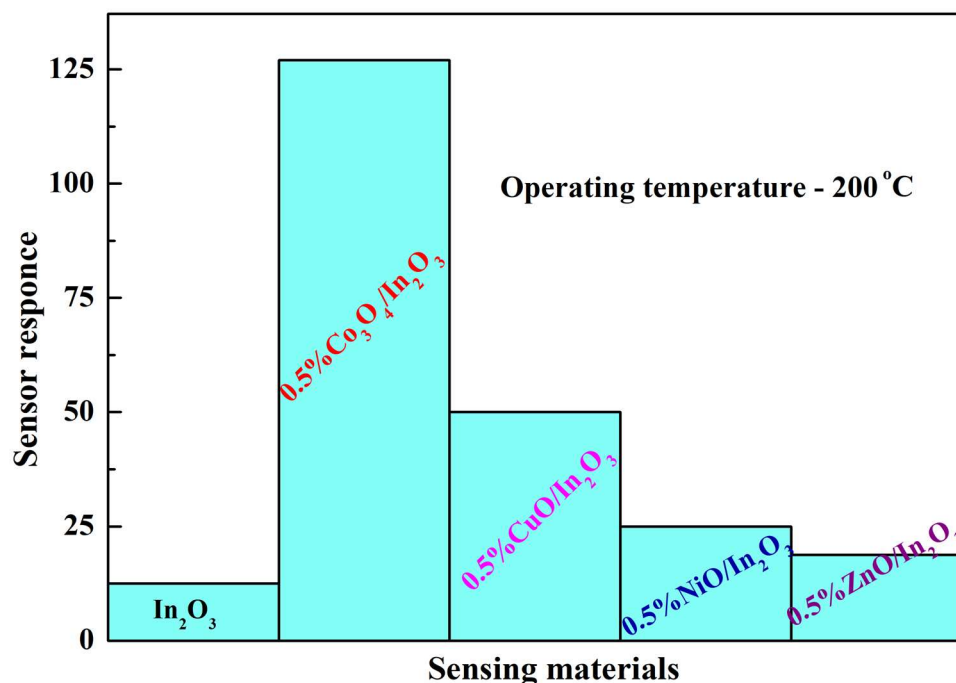


**Figure 2.** Sensor response of  $\text{In}_2\text{O}_3$ -based nanocomposites impregnated by various metal oxides in the detection of 1000 ppm CO.

The activity of  $\text{In}_2\text{O}_3$  doped with  $\text{Co}^{+2}$  ions is attributed to the fact that complexes of cobalt ions with oxygen vacancies are active centers of the sensor reaction [48]. The bonds of these ions with CO molecules [51] increase the adsorption of CO on such a complex.

### 2.1.2. Effect of Doping on Adsorption of Detected Gases

A change in the structure of metal oxide nanocrystals, due to their doping with metal oxides, leads to the formation of new adsorption centers. Two types of adsorption bonds between adsorbed organic molecules and metal oxide nanocrystals of the sensitive layer can be distinguished: acid–base bonds [52] and bonds between  $\pi$ -electrons of adsorbed molecules and d-electrons of metal ions in metal oxides [53,54].

Acid–base bonds are characteristic of adsorption on metal oxides with polar functional groups containing nitrogen or oxygen atoms. Doping of metal oxide nanocrystals with basic metal ions, including alkaline earth metal ions, creates adsorption centers for acidic compounds in their lattice. Such compounds are alcohols, aldehydes, ketones, etc., related to Brønsted acids [55,56]. Doping not only increases the number of adsorbed molecules but also can change the strength of their bond with nanocrystals, depending on the acidity of the molecules.

The influence of doping of  $\text{In}_2\text{O}_3$  nanocrystals with Ca, Sr, and Ba ions on sensor effects in the detection of formaldehyde, ethanol, and acetone by sensors based on these nanocrystals has been studied [57]. The sensor effect in the detection of formaldehyde decreases from Ca to Ba [55]. This is due to a drop in the electronegativity of metal ions and a decrease in their ability to attract electrons from the surrounding oxygen ions of an oxide. Their electron donation and the energy of bonds between the metal ions and adsorbed acid-type molecules also increase [58].

The sensor effect for  $\text{In}_2\text{O}_3$  nanocrystals doped with alkaline earth metal ions increases sharply [55] with an increase in the acidity of the analyzed compounds in the series acetone ( $\text{pK}_a = 20$ ), ethanol ( $\text{pK}_a = 15.9$ ), and formaldehyde ( $\text{pK}_a = 13.27$ ). Thus, there is a correlation between the acid–base bonds of the detected molecules with the sensitive layer and the magnitude of the sensor effect.

The nature of the adsorption bonds of  $\pi$ -electron molecules with a sensitive metal oxide layer depends on the electronic structure of the cations that make up this layer. Such bonds have been the most studied in relation to the CO molecule [59]. For effective detection, CO bonds with metal ions must be strong enough to ensure reliable CO adsorption on the surface of the sensor layer, at temperatures of 200–300 °C.

These bonds should not interfere with the sensor reaction of adsorbed molecules with oxygen active sites, mainly  $\text{O}^-$ . In this respect, the doping of oxides with divalent metal ions, in particular,  $\text{Mg}^{2+}$ ,  $\text{Mn}^{2+}$ ,  $\text{Fe}^{2+}$ ,  $\text{Co}^{2+}$ ,  $\text{Ni}^{2+}$ , and  $\text{Zn}^{2+}$ , which are characterized by reversible binding to CO molecules, is of particular interest [51]. Simultaneously, upon doping with these ions, oxygen vacancies appear in the system, which are the active centers of the sensor reaction. Ions in which d-electron shells are either absent ( $\text{Mg}^{2+}$ ) or completely filled ( $\text{Zn}^{2+}$ ) have the lowest binding energy with CO molecules. This bond is due to the electrostatic attraction between the metal ion and the lone pair of electrons of the  $5\sigma$  orbital of the C atom in the CO molecule; the energy of such a bond is about 8 kcal/mol [53,60].

When CO interacts with metal cations with unfilled d-electron shells ( $\text{Co}^{2+}$ ,  $\text{Ni}^{2+}$ ), the electron pair of the  $5\sigma$ -orbital of carbon is connected with the d-electrons of the metal. Concurrently, due to the overlapping of the unoccupied d-orbitals of the metal ion by the antibonding  $\pi^*$ -orbitals of CO, the  $\pi^*$ -d interaction appears [54]. This leads to an increase in the binding energy of the ion with CO, which, for  $\text{Co}^{2+}$  and  $\text{Ni}^{2+}$ , reaches about 13 kcal/mol [51].

In a series of CO sensors obtained by the hydrothermal method from indium oxide doped with  $\text{Cu}^{2+}$ ,  $\text{Pd}^{2+}$ , and  $\text{Ni}^{2+}$  ions, sensors containing  $\text{Ni}^{2+}$  have the highest sensor effect, which is six times the effect in the absence of additives [61]. Doping of  $\text{In}_2\text{O}_3$  with  $\text{Zn}^{2+}$  ions also increases the sensor effect approximately 3.5 times [62].

A similar effect of the interaction energy of CO with doping ions on the sensor effect was observed in sensors based on  $\text{SnO}_2$  doped with  $\text{Zn}^{2+}$  and  $\text{Ni}^{2+}$  ions [63]. Thus, as in systems with acid–base bonds between the analyzed gas and the sensitive layer, an increase in the energy of CO adsorption bonds, due to the  $\pi^*$ -d interaction of CO with doping ions, causes an increase in the sensor effect.

### 2.1.3. Influence of the Nature of Doping Ions on the Reactivity of Oxygen Anionic Centers

In the reactions of anions localized on the surface of a metal oxide sensitive layer, the activation energy that determines the sensor effect depends on the binding energy of the anion with the metal oxide. The effect of these bonds was demonstrated in the detection of formaldehyde by a sensor based on  $\text{In}_2\text{O}_3$ , doped with ions of various metals [64–66]. The Fermi level (see Figure 3) of the sensitive layer increased or decreased depending on the nature of the doping ions.

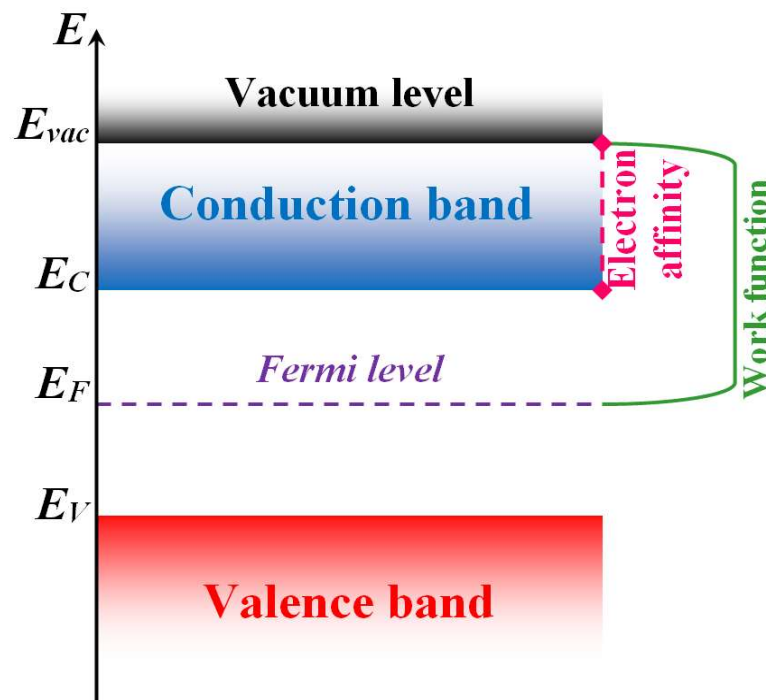


**Figure 3.** Semiconductor band structure. Here,  $E_{vac}$  is minimal vacuum energy of electron,  $E_C$  is bottom of the conduction band,  $E_F$  is Fermi level and  $E_V$  is valence band ceiling.

An increase in the Fermi level leads to an increase in the sensor effect in the detection of formaldehyde and other reducing compounds [59]. This trend can be attributed to the increase in the reactivity of active oxygen anions, due to a reduction in their binding energy to the surface. The reduced binding energy is caused by a decrease in the electron affinity  $\chi_e$  of the metal oxide sensitive layer from the increase in the Fermi level.

An increase in the Fermi level of the sensitive layer leads to the increase in the concentration of adsorbed oxygen anions. The change in concentration is due to the difference between the Fermi level of the metal oxide and the energy of electrons captured by adsorbed oxygen atoms or molecules, as well as the increase in the number of electrons passing from the semiconductor to oxygen, to achieve equilibrium. An increase in  $\chi_e$ , on the contrary, causes a decrease in the sensor effect [64]. A similar dependence of the sensor effect on the Fermi level (and  $\chi_e$ ) of the sensitive layer was observed in [55,57].

The influence of the metal oxide layer on the reactivity of the active oxygen particles associated with this layer was considered, as well as the dependence on the average characteristics, such as the electron affinity related to the entire layer [64]. In reality, oxygen molecules are adsorbed on certain lattice defects, where the coordination between metal ions and oxygen ions of the metal oxide lattice is disrupted. In this case, bonds of coordinating-unsaturated metal ions with environmental molecules can be formed. Essentially, such defects are oxygen vacancies [44], whose properties depend on the structure of the crystal lattice and the location of the vacancy. Accordingly, the chemical activity of a vacancy in the sensor process is changed [67].

The properties of vacancies depend on the conditions of metal oxide annealing during the formation of the sensitive layer. Thus, nanocrystalline SnO<sub>2</sub>, obtained by the hydrothermal method of tin hydroxide annealing, contains both isolated oxygen vacancies and clusters of oxygen vacancies, in combination with vacancies of tin ions [68]. The number of vacancies and the ratio between vacancies of different types depends on the medium in which the annealing is carried out—in air, in oxygen, or in helium. In accordance with this, the sensor response to acetone, ethanol, and formaldehyde is changed [68].

As noted in the previous section, the chemical activity of the metal oxide, and the sensor effect in the detection of reducing agents, increase with a decrease in the bond energy between oxygen ions and metal ions. To clarify this mechanism, the sensitivity of MnO<sub>2</sub> nanofibers doped with niobium ions to CO was studied [69]. The Mn–O–Nb sequences formed in doped nanofibers contain oxygen ions weakly bound with the ions of these metals. Therefore, the reaction,  $\text{CO} + \text{Mn–O–Nb} \rightarrow \text{CO}_2 + \text{Mn–V}_\text{O}\text{–Nb}$ , with the formation of oxygen vacancies (V<sub>O</sub>) proceeds efficiently, even at room temperature. This reaction leads to a sharp drop in the resistance of nanofibers, but the reasons for this are not discussed in [69].

It can be assumed that, since the electron levels of the formed vacancies lie near the conduction band of the nanofibers [44,65], electrons from oxygen vacancies easily pass into them. As a result, the conductivity of the composite increases, leading to a sensor effect. After replacing the air mixture, with CO, with pure air, the vacancies are filled with oxygen, and the resistance of the sensor system returns to its original value.

This system has exceptionally high sensitivity to CO, which makes it possible to detect the gas, even at its concentration in air of 2 ppm [69]. A high selectivity of CO detection is thus achieved in the presence of organic compounds, which can be explained by the selective adsorption of CO on Mn–O–Nb structures [70]. These structures are very stable. Therefore, the formation of oxygen vacancies under the influence of CO and their death upon interaction with oxygen are completely reversible processes.

A similar increase in the reactivity of oxygen ions was found for cerium oxide doped with samarium ions [71]. The Ce–O–Sm structures formed in this material also contain labile oxygen ions weakly bonded to the lattice. As a result, the rate of CO oxidation with the formation of oxygen vacancies increases, and the maximum of oxidative activity shifts to lower temperatures. All this testifies to the key role of oxygen vacancies and complexes of vacancies with metal ions in the sensor process.

## 2.2. Mechanisms for Increasing Sensitivity of Two-Component, Two-Phase Metal Oxide Composites

In contrast to single-phase systems, different conduction paths are formed in binary two-phase systems, by aggregates of component particles contacting with each other. Below, we consider the influence of the nature and structure of conduction pathways, as well as the interaction between components, on the conductivity and sensor properties of nanocomposites. The mechanisms of chemical and electronic sensitization of sensor processes are also discussed.

### 2.2.1. Effect of Conduction Pathways on Sensor Properties of Binary Two-Phase Nanocomposites

The conductivity of the sensor layer is determined by the aggregates of metal oxide particles that are in contact with each other and form current flow paths. In a two-component system, in which components A and B form different crystalline phases, there are three types of intercrystalline contacts, namely homophase contacts A–A and B–B, and heterophase contacts A–B. As a rule, nanoparticles A and B have different work functions (*W*), such that, upon their contact, electron transfer occurs at  $W_A > W_B$  from B to A, and at  $W_B > W_A$ , in the opposite direction. Such an electron transfer between nanoparticles corresponds to their mutual charging [27].

An internal electric field develops at heterogeneous contacts. In this case, the potential barrier, that prevents the passage of current through a heterogeneous contact between

particles, depends on the mutual direction of the internal and external fields [72]. In a disordered system of nanoparticles, which includes heterogeneous contacts, when the direction of the external field is opposite to the direction of the field in the contact, high barriers inevitably arise on the current path. The current flow path “bypasses” such contacts, choosing the homogeneous contacts with lower barriers for electron transfer [72].

Thus, in two-phase nanocomposites consisting of particles of components A and B, two parallel homophase conduction paths can be realized through the contacting nanoparticles A-A or B-B. The current flows through chains of contacting nanoparticles, which form conducting clusters that connect the electrodes of the measuring system (“endless” clusters [72,73]). The nanoparticles of the second component, that did not enter the conduction pathways, are modifiers, the interaction with which changes the chemical and electronic characteristics of the conducting nanocrystals, and, consequently, the conductivity and sensor effects.

In a disordered two-phase conglomerate from particles of two components, the conduction paths are determined by percolation theory [73], and depend on the relative content of the components and the ratio between the sizes of the corresponding nanocrystals [72].

In nanostructured composites ranging from *n*- and *p*-modifications of TiO<sub>2</sub>, three conduction regions are possible [72], based on the percolation model, depending on the relative content of the components. These are regions I and II, with conducting clusters of nanoparticles of only one type, and region III, in which conducting clusters of both types coexist. In region III, the conductivity of the composite depends on the ratio between the concentrations of components, the size of the particles, and the concentration of current carriers (electrons or holes) in the components [72].

In a nanostructured composite of metal oxides with different work functions, the magnitude and direction of the sensor effect are determined by the electron transfer between the conducting clusters and the modifier. A characteristic example is the result obtained from the study of the conductivity and sensor effect in a composite of SnO<sub>2</sub> nanofibers with nanoclusters of TiO<sub>2</sub> or WO<sub>3</sub> modifiers located on the surface of the nanofibers [74]. In SnO<sub>2</sub> nanofibers and modifier nanoclusters, the work function is different; therefore, the effect of modifiers on conductivity and sensor properties depends on the difference between the  $W_{\text{SnO}_2}$  and  $W$  of the modifier. Modification of nanofibers with TiO<sub>2</sub> nanoclusters ( $W_{\text{TiO}_2} < W_{\text{SnO}_2}$ ) leads to an increase in the conductivity of the composite, due to electron transfer from TiO<sub>2</sub> to SnO<sub>2</sub>, while modification with WO<sub>3</sub> nanoclusters ( $W_{\text{WO}_3} > W_{\text{SnO}_2}$ ) reduces the conductivity, due to electron transfer from SnO<sub>2</sub> to WO<sub>3</sub> [74].

The modification of SnO<sub>2</sub> nanofibers also changes sensor effects, in addition to the conductivity. An increase in conductivity under the influence of TiO<sub>2</sub> causes an increase in the sensor effect for oxidizing gases but has almost no effect on the sensor effect for reducing agents. The decrease in conductivity caused by WO<sub>3</sub> nanoclusters also leads to an increase in the sensor effect in the detection of reducing gases [74].

A similar increase in the sensor response to reducing gases, accompanied by a decrease in the conductivity of the composite, is observed for the deposition of WO<sub>3</sub> nanoclusters on the surface of In<sub>2</sub>O<sub>3</sub> nanofibers. In contrast, the deposition of In<sub>2</sub>O<sub>3</sub> on WO<sub>3</sub> nanofibers increases their conductivity and sensor response to oxidizing gases but reduces the sensitivity of the composite to reducing agents [75].

In numerous reviews on two-phase nanocomposites (see, for example, [76,77]), as in the studies considered above, only systems with conduction paths from particles of one component are mostly discussed. Particles of the second component, interacting with conductive particles, change their properties and affect sensor effects.

Binary nanocomposites with different conduction paths have different sensitivity to detected gases. The authors of [78,79] studied systems consisting of metal or metal oxide nanoparticles in combination with thin nanolayers of reduced graphene oxide (rGO). With minimal coverage of rGO layers by Pd particles, these layers are current flow paths, and the conductivity decreases in the presence of hydrogen. This is due to the transformation of Pd

nanoparticles into PdH<sub>x</sub>, followed by electron transfer from PdH<sub>x</sub> to rGO and a decrease in the concentration of charge carriers—holes in the *p*-semiconductor rGO [78].

With an increase in the concentration of Pd particles, the response to H<sub>2</sub> decreases, due to a change in the conduction paths—from rGO layers to clusters of Pd nanoparticles. This occurs during the formation of a continuous Pd film on the surface of the rGO layers. Due to the change in the structure of the Pd film, under the influence of hydrogen dissolved in it, the response increases [78]. In the absence of Pd nanoparticles, the conductivity of rGO layers largely does not react to the presence of nonpolar molecules in the air, for example, H<sub>2</sub>. The effect of current flow paths in nanocomposites combining rGO layers with metal oxide nanoparticles on conductivity and sensor properties was studied in detail using the response to ammonia as an example [80].

As rGO was added to nanostructured SnO<sub>2</sub>, the type of conductivity of the composite changed from electronic conductivity, characteristic of pure SnO<sub>2</sub>, to hole conductivity, characteristic of rGO. Due to the difference in the shape of the components (thin, extended rGO nanolayers and quasi-spherical SnO<sub>2</sub> nanoparticles), the percolation transition from *n*- to *p*-composites occurs already at small (about 0.5 wt.%) additions of rGO to SnO<sub>2</sub>.

These experimental results agree with the calculations [80]. The response of the sensor to ammonia is due to its reaction with oxygen anions on the surface of SnO<sub>2</sub> particles. In *n*-type nanocomposites, where the current flows through clusters of SnO<sub>2</sub> nanoparticles, the addition of ~0.5 wt.% rGO leads to an increase in the electronic conductivity of the composite [80]. Since  $W_{\text{rGO}}$  (5.2 eV) of a completely reduced graphene oxide film [81] is larger than  $W_{\text{SnO}_2}$  (4.9 eV), electrons pass from SnO<sub>2</sub> to rGO. As a result, the electron concentration in conducting clusters of SnO<sub>2</sub> nanoparticles decreases, which increases the response to reducing gases [74,82].

In connection with the mutual charging of contacting SnO<sub>2</sub> nanoparticles and rGO nanolayers, during the transition of electrons from SnO<sub>2</sub> to rGO, favorable conditions are created for the adsorption of polar molecules in the contact region in the nanocomposite. This also applies to NH<sub>3</sub> molecules and additionally increases the sensitivity of the composite sensor to ammonia. An increase in rGO concentration to 1 wt.% leads to a percolation transition from conduction through SnO<sub>2</sub> particles to conduction paths through rGO layers; that is, to hole conduction [80].

The paths of hole and electron conduction are different in nanostructured metal oxides [3,77,83]. The electron current flows through contacting nanoparticles, crossing their surface layers where potential barriers are formed between the particles, due to oxygen ionosorption accompanied by the capture of electrons from the conduction band. The resistance of the surface layers is significantly increased, compared to the resistance in the bulk of the particles. The height of such barriers on the current path is determined by the number of electrons captured by oxygen, which decreases when O<sup>−</sup> interacts with a reducing gas. This leads to an increase in conductivity.

In the case of hole conduction, the current flows mainly in the near-surface layers of *p*-nanoparticles, wherein, the negative charge of O<sup>−</sup> on the surface is compensated by the positive charge of holes in the near-surface layer. The concentration of holes in this layer is naturally higher than in the volume of the particles [83,84]. The total resistance to the hole current in the volume of the particles and surface layers is determined by the morphology of the nanostructured metal oxide [85].

At the hole conduction, the total resistance ( $R_{\text{sen}}$ ) of the sensor layer includes a volume component which is largely independent of the processes on the particle surface. Therefore, the sensitivity to reducing gases in such systems is significantly less than in the case of electronic conduction, when the change in resistance is determined by the reactions of the analyzed gases with O<sup>−</sup> on the surface of the particles. SnO<sub>2</sub>-rGO sensors to ammonia, with hole conduction along the paths formed by rGO layers, are characterized by greater stability and a shorter response time to ammonia, and relaxation time after its removal [80].

The conductivity and sensor properties of nanocomposite fibers containing *n*-SnO<sub>2</sub> and *p*-Co<sub>3</sub>O<sub>4</sub> nanoparticles were studied in [23]. The resistance of the  $x\text{SnO}_2 - (1 - x)\text{Co}_3\text{O}_4$

system and its sensor response to CO, C<sub>6</sub>H<sub>6</sub>, and C<sub>3</sub>H<sub>6</sub>O reach their maximum values at  $x = 0.5$ . The nanofiber of this composition has electronic conductivity. Since the arrangement of nanoparticles in a fiber is chaotic, the conductivity of a nanocomposite fiber is determined by the percolation model [72,73].

According to this model, the electron current in such a system flows along *n*-type homophase paths, excluding heterophase *n-p* contacts, the inclusion of which in the current path would lead to the occurrence of large potential barriers. Heterophase contacts between *n*- and *p*-nanoparticles of composite lead to the loss of electrons, due to electron-hole recombination. As a result, the electron concentration in the conducting channels decreases. In some cases, this leads to an increase in the response to reducing gases [83].

Similar effects are also characteristic of other *n-p* nanocomposites [86,87], in which the maximum response is achieved in the systems with electronic conductivity. The sensitization of the sensor response by *p*-nanoparticles contacting with *n*-nanoparticles of conducting pathways is due to a decrease in the electron concentration in conducting pathways, resulting from electron-hole recombination. At *n-n*-contacts, the concentration of conduction electrons does not decrease, but the electrons pass into a lower-energy conductivity band, forming an “accumulation layer” of electrons in acceptor centers [83,88]. Such a transition also reduces the concentration of conduction electrons in the conducting paths of the composite, but to a lesser extent since the transition of electrons is hindered by the resulting electric field. Therefore, *n-p* contacts are more effective for sensitizing the composites undergoing the electronic conductivity.

#### 2.2.2. Effect of Interaction between Conducting and Modifying Nanocrystals on Sensor Properties of a Composite

In binary systems, the interaction of nanoparticles, constituting current flow paths with modifier nanoparticles surrounding these paths, is a source of sensor sensitization. There are two types of sensitizations: chemical and electronic [13,89].

Chemical sensitization is caused by catalytically active particles of the modifier, which chemisorb oxygen and molecules of detected gases with the formation of reactive particles, in particular, atoms or radicals. The most common variant of chemical sensitization is the adsorption and dissociation of oxygen molecules on modifier particles with a subsequent spillover of oxygen atoms into conducting clusters. After that, oxygen atoms capture electrons from the conduction band of nanoparticles constituting conducting clusters, forming O<sup>−</sup> radical anions.

Since the reaction of reducing gases with O<sup>−</sup> on the surface of conducting clusters “releases” trapped electrons and increases the conductivity of the composite, the concentration of adsorbed oxygen should be increased to raise the sensitivity. This is clearly facilitated by the catalytic activity of modifier nanoparticles [14,90].

The detection of several  $\pi$ -electron compounds, by sensors based on SnO<sub>2</sub> nanofibers modified with Au, Pd, and Pt nanocrystalline particles, was studied to determine the optimal conditions for achieving the maximum sensitivity [91]. The study indicated that the adsorption bonds, of  $\pi$ -electron molecules with metal particles, are determined by the location of the metal d-electron band, relative to the  $\pi$ -electron orbitals of the molecules of the analyzed gases. Therefore, by varying the electronic structure of the contact between a gas molecule and a metal particle on the surface of SnO<sub>2</sub> nanofibers, chemisorption can be increased. The spillover of adsorbed molecules from metal particles onto SnO<sub>2</sub> fibers increases the gas concentration on nanofibers and the sensitivity of the composite. The conditions were determined for the most efficient chemical sensitization of the sensor effect by Au, Pd, and Pt particles in the detection of CO, benzene, and toluene [91].

Chemical sensitization depends both on the structure of the detected molecule and the properties of the catalytically active particle. A typical example is the sensitization of CO and H<sub>2</sub> detection by a sensor based on nanocrystalline In<sub>2</sub>O<sub>3</sub>, containing nanoparticles of the well-known catalyst, ZrO<sub>2</sub>. The particles of ZrO<sub>2</sub> increase the sensor effects in the detection of H<sub>2</sub>, but practically, do not affect the detection of CO [92].

The effect of chemical sensitization of the sensor response to CO on this system could be expected, due to the dissociation of O<sub>2</sub> on the surface of ZrO<sub>2</sub> nanoparticles with the subsequent formation of O<sup>−</sup> active centers. However, the dissociation of O<sub>2</sub> requires a temperature above 800 °C [93]. The efficiency of H<sub>2</sub> detection is probably ensured by the dissociation of H<sub>2</sub> molecules under the influence of ZrO<sub>2</sub>. As a result of the spillover of the formed hydrogen atoms onto In<sub>2</sub>O<sub>3</sub> particles, H atoms react with O<sup>−</sup> radical anions localized on the In<sub>2</sub>O<sub>3</sub>. In this case, the electrons captured by oxygen return to In<sub>2</sub>O<sub>3</sub>.

The conductivity of a nanofiber network is determined by potential barriers to electron transfer between contacting nanofibers, and depends on the electron concentration in their surface layers ( $n_s$ ) [83]. The decoration of SnO<sub>2</sub> fibers, with electron-donating TiO<sub>2</sub> ( $W_{\text{TiO}_2} < W_{\text{SnO}_2}$ ) or electron-withdrawing WO<sub>3</sub> ( $W_{\text{WO}_3} > W_{\text{SnO}_2}$ ) nanoclusters, leads to a redistribution of conduction electrons between conducting channels and decorating clusters [74]. The transfer of electrons from SnO<sub>2</sub> nanofibers to WO<sub>3</sub> nanoclusters reduces  $n_s$  and increases the barriers for electron transfer between contacting nanofibers [83]. All this affects the sensor effect [68], and can be considered as electronic sensitization.

The sensor properties of nanocomposites depend on the method of their formation, which determines their morphology. In this regard, the indicators are the results of studies of composites obtained by physical mixing of oxide nanopowders or by laser sputtering of one oxide on the surface of crystals of another [21,22,94–96]. In such composites based on electron acceptor SnO<sub>2</sub> or ZnO oxides, electron-donating additives of In<sub>2</sub>O<sub>3</sub> or TiO<sub>2</sub> nanoparticles do not decrease the sensor effect for reducing gases, as in [74,97,98], but increase it.

It should be noted that the sensor characteristics of binary composites obtained by mixing nanocrystalline powders, in contrast to the systems considered in [74,97,98], are mainly determined by the contact of particles with different electron affinities and clearly marked interphase boundaries [94], where the charges, formed as a result of mutual charging of such particles, are localized. Charges in the interfacial regions of the nanocomposite, as mentioned above [80], can increase the chemisorption of oxygen and detected gases and, thus, increase the sensor effect.

The effect of interfacial contacts on the sensor properties of nanocomposites was not considered in [74,75]. This is probably due to the small size of electron-donor and electron-acceptor clusters located on the surface of conducting nanofibers, because of which, the distribution of electrons in the region of these contacts is largely blurred.

It can be assumed that the differences in the sensor properties of nanocomposites obtained by different methods are due to the structure of the interfacial regions in such composites, which determines the adsorption of gases and their activity in sensor reactions. The largest increase in the sensor effect is achieved due to the joint effect of chemical and electronic sensitization by chemically active modifiers with a high work function [90].

Such sensitization of the sensor effect occurs, in particular, as a result of the modification of the surface of conducting metal oxide particles by nanoclusters of catalytically active metals, Au, Pd, and Pt [91]. Nanoclusters of these metals, as shown above, catalyze the formation of highly reactive atoms and radicals on the surface of metal oxide nanocrystals, which corresponds to chemical sensitization. These nanoclusters, which have a higher work function than conductive metal oxide nanocrystals, capture the electrons of the nanocrystals, lowering  $n_s$ . Thus, there is also an electronic sensitization of the sensor effect.

A characteristic example of the synergism of electronic and chemical sensitization is the detection of ethanol vapor by sensors based on In<sub>2</sub>O<sub>3</sub> nanotubes, decorated by nanoclusters, Co<sub>3</sub>O<sub>4</sub>, Fe<sub>2</sub>O<sub>3</sub> or a combination of these nanoclusters [99]. The deposition of nanoclusters, of even a single metal oxide on the surface of nanotubes, increases the sensor effect due to electron sensitization, since the work function of these metal oxides is higher than that of In<sub>2</sub>O<sub>3</sub>. In this case, Co<sub>3</sub>O<sub>4</sub> clusters have a greater influence, although  $W$  for Fe<sub>2</sub>O<sub>3</sub> (5.3 eV [100]) is higher than for Co<sub>3</sub>O<sub>4</sub> (4.8 eV [101]).

Co<sub>3</sub>O<sub>4</sub> nanoclusters are both electronic and chemical sensitizers, which is due to the catalytic activity of Co<sub>3</sub>O<sub>4</sub> in the dissociation reactions of adsorbed oxygen molecules with the formation of O<sup>-</sup>. The largest increase in the sensor effect occurs with the joint application of Co<sub>3</sub>O<sub>4</sub> and Fe<sub>2</sub>O<sub>3</sub>, when high chemical sensitization of the sensor effect under the action of Co<sub>3</sub>O<sub>4</sub> is combined with high electronic sensitization under the influence of Fe<sub>2</sub>O<sub>3</sub> [99].

The synergism of the sensitizing action of different agents is also manifested in sensors based on porous In<sub>2</sub>O<sub>3</sub> nanospheres, modified with NiO and Au nanoclusters [102]. The interaction of NiO clusters with In<sub>2</sub>O<sub>3</sub> leads to the formation of oxygen vacancies on the surface of In<sub>2</sub>O<sub>3</sub> in such systems, due to the difference in the charges of Ni<sup>+2</sup> and In<sup>+3</sup> ions. Concurrently, Au nanoclusters catalyze the dissociation of these molecules, with the capture of electrons and the formation of O<sup>-</sup> active centers.

The combined action of NiO and Au clusters on In<sub>2</sub>O<sub>3</sub> nanoparticles produces high sensitivity in the detection of reducing compounds, in particular, toluene [102]. Using such a sensor, toluene can be detected, even at concentrations of the order of 100 ppb, since Au clusters adsorb toluene and thus increase the sensor effect. A similar synergistic effect of electronic and chemical sensitization of the sensor effect was also found for In<sub>2</sub>O<sub>3</sub> nanotubes containing NiO and PdO nanoclusters on the surface [39].

The results presented in this section have shown that the sensor response for two-component, two-phase metal oxide composites can differ markedly for various gases. Table 1 summarizes the results of previous investigations and makes it possible to compare the response magnitudes to various gases of sensors synthesized with different methods under diverse conditions.

**Table 1.** Sensor response to various gases of two-component two-phase metal oxide composites.

Material	Synthesis Method	Sensor Response (Gas Concentration)	Temperature	References
0.5SnO <sub>2</sub> -0.5Co <sub>3</sub> O <sub>4</sub>	electrospinning method	18.7 (1 ppm C <sub>6</sub> H <sub>6</sub> )	350 °C	[23]
WO <sub>3</sub> -SnO <sub>2</sub>	sputtering high-purity Ti or W targets on SnO <sub>2</sub>	140 (1 ppm H <sub>2</sub> )	300 °C	[74]
TiO-SnO <sub>2</sub>		232 (1 ppm O <sub>2</sub> )		
WO <sub>3</sub> -In <sub>2</sub> O <sub>3</sub>	sol-gel method	27 (200 ppm NO <sub>2</sub> )	300 °C	[75]
graphene-Pd/SnO <sub>2</sub> composites	grapheme by CVD method, SnO <sub>2</sub> gas phase synthesis method	14.8% (1% C <sub>2</sub> H <sub>5</sub> OH)	200 °C	[79]
rGO-SnO <sub>2</sub>	rGO by hydrothermal treatment of aqueous dispersion of GO, rGO-SnO <sub>2</sub> composite by mixing	1.3 (50 ppm NH <sub>3</sub> )	22 °C	[80]
0.5SnO <sub>2</sub> -0.5NiO	electrospinning process	36 (10 ppm NO <sub>2</sub> )	300 °C	[86]
SnO <sub>2</sub> -2.78CuO	sol-gel route	200% (400 ppm CO)	350 °C	[87]
In <sub>2</sub> O <sub>3</sub> -Co <sub>3</sub> O <sub>4</sub>	Electrospinning method	39 (200 ppm HCHO)	260 °C	[88]
Pt-SnO <sub>2</sub>	photolithographic process and γ-ray radiolysis method	40 (1 ppm C <sub>7</sub> H <sub>8</sub> )	300 °C	[91]
10%Co <sub>3</sub> O <sub>4</sub> -90% In <sub>2</sub> O <sub>3</sub>	Mixing metal oxides	1300 (1100 ppm H <sub>2</sub> )	250 °C	[92]
20%ZrO-80% In <sub>2</sub> O <sub>3</sub>		280 (1100 ppm H <sub>2</sub> )	315 °C	
TiO <sub>2</sub> /SnO <sub>2</sub>	hydrothermal process	52.3 (100 ppm triethylamine)	260 °C	[96]
ZnO@In <sub>2</sub> O <sub>3</sub>	hydrothermal method	28.6 (100 ppm C <sub>2</sub> H <sub>5</sub> OH)	160 °C	[97]
Au-NiO/In <sub>2</sub> O <sub>3</sub>	solvothelmal method	80.6 (10 ppm toluene)	250 °C	[102]

The consideration of the processes of chemical and electronic sensitization of sensor reactions has shown that such a division is rather arbitrary. For example, oxygen molecules dissociate on the surface of nanoparticles with the formation of chemically active

centers, which corresponds to chemical sensitization, wherein, the formed oxygen atoms actively capture electrons from the near-surface layer, thereby depleting it; this is already characteristic of electron sensitization. Thus, in various sensor processes, both types of sensitization mechanisms can occur simultaneously, but the chemical or electronic nature will be manifested to a greater extent.

### 2.3. Interaction of Nanocomponents in Core–Shell Sensor Systems

Two-phase structures of the core–shell type have been intensively studied in the last decade. Such structures consist of a core of metal oxide covered by a layer of another semiconductor oxide (see, for example, reviews [14,103–106]).

With the right choice of core and shell materials, such structures can achieve exceptionally high sensitivity and selectivity in the detection of various substances. This also makes it possible to significantly lower their operating temperature [14,104,105,107–109]. These materials have generally different morphologies, but the highest sensitivity is exhibited by structures formed by composite nanofibers (see Figure 4). The sensor characteristics of such a material depend on the path of current flow. According to the percolation model of conductivity in a disordered system of semiconductor particles with different electron work functions [72,73], the current in the sensitive layer passes through the fiber shell, overcoming the barriers of the homocontacts, but bypassing the potential barriers of heterocontacts in the core–shell system [110].

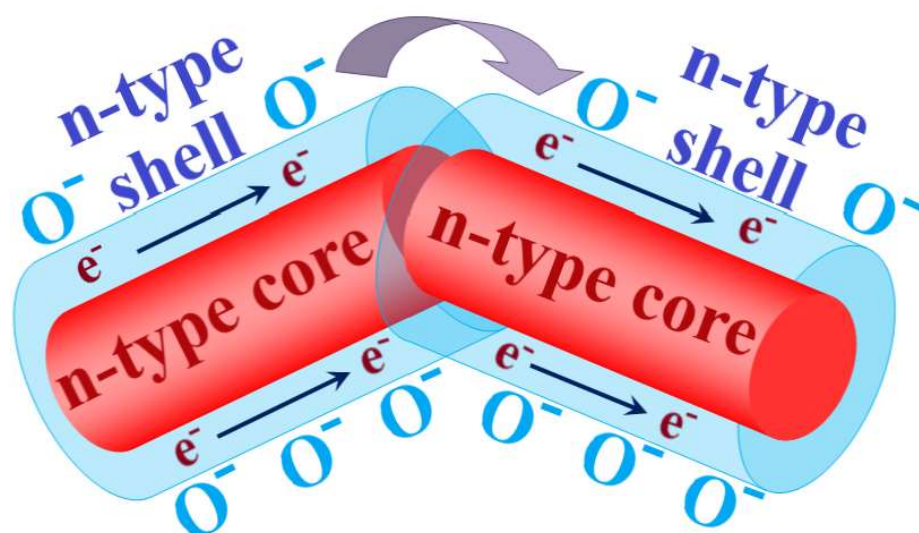


**Figure 4.** Scheme of the sensitive layer of composite nanofibers of the core–shell type. « $e^- \rightarrow e^-$ » indicates the current flow in the shell of nanofibers.

Such a scheme has been confirmed by the results obtained from the detection of a reducing agent (benzene) and an oxidizing agent ( $\text{NO}_2$ ) by composites of  $n\text{-ZnO-p-CuO}$  nanofibers [111] (here and hereinafter, the first oxide is the core, and the second is the shell). The conductometric sensor response to these compounds in the sensitive layer of  $n\text{-ZnO-p-CuO}$  nanofibers indicates hole conductivity through the nanofiber shells without crossing the fibers. In this case, the value of the sensor response, due to the features of hole conductivity [112], is much lower than in the sensitive layer from pure zinc oxide nanofibers with electronic conductivity [111]. An increase in the sensor response, when  $p\text{-CuO}$  nanoparticles are included in such a layer, is due to a change in the electronic conductivity as a result of contacts between  $n\text{-ZnO}$  and  $p\text{-CuO}$  nanoparticles and electron transfer from ZnO to CuO.

The resistance of the sensitive layer, as in other nanostructured metal oxide semiconductors, is determined by the resistance of contacts between nanoparticles (in this case, nanofibers), which in systems with electronic conductivity increases with a decrease in the electron concentration in the shells.

Two factors affect the concentration of electrons in the shell nanofiber. The first factor is the capture and localization of conduction electrons by electron-withdrawing centers on the outer and inner surfaces of the shell, which leads to the depletion of the shell in electrons. On the outer surface, such centers are adsorbed forms of oxygen, which, at the “operating” temperatures of the sensors above 200 °C, are mainly oxygen atoms. On the inner surface separating the nanofiber shell from the core, electrons are trapped by lattice defects that arise during the formation of the composite, due to the difference in the structures of the core and shell [113].

Another factor is associated with the presence of electron heterojunctions between the core and shell. Such a transition is determined by the difference in the values of the electron work function  $W$  for the core  $W_C$  and the shell  $W_{Sh}$  of the fiber. If  $W_{Sh} < W_C$ , conduction electrons pass from the shell to the core. In this case, the shell of the composite fiber is even more depleted of electrons.

According to existing concepts, the most promising are sensors based on core–shell nanofibers, which contain weakly conductive catalytically active layers of  $\text{SnO}_2$  or  $\text{ZnO}$ . Modification of core–shell metal oxide systems with noble metal nanoparticles can have a significant effect on their sensor response and selectivity. Sensors based on such nanofibers make it possible to detect even traces of various organic compounds in the air (see, for example, [114–117]).

The response to 0.1 ppm CO of core–shell sensors, based on  $\text{SnO}_2$ - $\text{ZnO}$  nanofibers with Au nanoclusters located on the surface of  $\text{ZnO}$  shells, is 25, while for pure  $\text{SnO}_2$  and  $\text{ZnO}$  nanofibers, it is only 3 and 2, respectively [114,118]. The maximum sensor response in the detection of 100 ppb benzene, by  $\text{SnO}_2$ - $\text{ZnO}$  nanofibers with Pd nanoclusters on the surface of  $\text{ZnO}$  shell, is 71 [116]. This is much higher than the sensor effect for  $\text{SnO}_2$  (1.9) and  $\text{ZnO}$  (2.1) nanofibers, as well as for  $\text{SnO}_2$ - $\text{ZnO}$  sensors that do not contain Pd clusters (11.2). It is also interesting that the deposition of silver nanoparticles on the surface of a nanosystem consisting of tungsten oxide ( $\text{W}_{18}\text{O}_{49}$ ), included in a polypyrrole shell, leads to an increase in the sensor response to ammonia and an improvement in the selectivity of this system [115].

To determine the mechanism of sensor effects in composite nanofibers, it is important to find out how the electrical and sensor characteristics of fibers change when the material of the core and shell are swapped. Sensor effects in the detection of CO and aromatic hydrocarbons were determined for core–shell  $\text{ZnO}$ - $\text{SnO}_2$  nanofibers [118]. A comparison with data for similar layers of  $\text{SnO}_2$ - $\text{ZnO}$  nanofibers [109] makes it possible to elucidate important features of the resistance and sensor effects in these systems.

In both cases, shells were formed on monocrystal nanorods by deposition of atomic layers. According to [108,109], the interaction between the core and shell in  $\text{SnO}_2$ - $\text{ZnO}$  nanofibers leads to an increase in the resistance of the sensor system, due to the contacts between the layers. The sensor effect is also increased.

The values of resistance and the sensor effect of core–shell composites largely depend on the thickness of the shell. For the  $\text{SnO}_2$ - $\text{ZnO}$  nanocomposite, the maximum values of these parameters are achieved at a shell thickness of about 30 nm; that is, close to the Debye charge screening length in  $\text{ZnO}$  ( $\lambda_{\text{ZnO}}$ ), which is 22–35 nm [116]. A similar dependence on the shell thickness was also observed in another sensor system of the same type.

The maximum sensor response of the  $\text{Nb}_2\text{O}_5$ - $\text{ZnO}$  system of the core–shell type to 1%  $\text{H}_2$  at 300 °C is observed at a  $\text{ZnO}$  shell thickness of about 50 nm, which is close to  $2\lambda_{\text{ZnO}}$  [119]. These data indicate the presence of electron-withdrawing defects in the  $\text{Nb}_2\text{O}_5$ - $\text{ZnO}$  system at the interface core–shell, which reduce the electron concentration in the shell. Therefore, the length of the screening of charges on oxygen centers, formed on the surface of the shell during oxygen chemisorption, increases. Meanwhile, the reaction of these centers with the analyzed reducing agent and the “release” of trapped electrons, respectively, causes a sensor response, as evidenced by an increase in conductivity.

Judging by the data on the resistance of  $\text{SnO}_2$ - $\text{ZnO}$  and  $\text{ZnO}$ - $\text{SnO}_2$  nanofiber layers [114,117], the concentration of conduction electrons in the shells of these nanofibers

decreases mainly due to defects at the boundary between SnO<sub>2</sub> and ZnO. The transfer of electrons between SnO<sub>2</sub> and ZnO increases or decreases the electron concentration in the shells, depending on which of these materials forms the core or shell of the nanofibers. The value of the sensor effect, in the detection of reducing compounds (CO, C<sub>6</sub>H<sub>6</sub>, C<sub>7</sub>H<sub>8</sub>) by SnO<sub>2</sub>-ZnO and ZnO-SnO<sub>2</sub> sensors, changes according to the change in the resistance of the sensitive layer [114,117].

The attribution of the large value of the sensor effect in core-shell nanofibers, when both the core and the shell have catalytic activity, to only the influence of the system resistance, is not sufficiently substantiated. Indeed, in [116–118], a significant increase in the sensor effect was observed when nanoclusters of noble metals were located on the surface of shells, although such additives only reduce the resistance of the film. In addition, a very noticeable sensitivity and selectivity was found in the detection of ethanol by In<sub>2</sub>O<sub>3</sub>-ZnO nanofibers [120] containing In<sub>2</sub>O<sub>3</sub> core with a very high electron concentration, which can pass into the ZnO shell, since the work function of the electron for In<sub>2</sub>O<sub>3</sub> is lower than for ZnO. The sensor effect for composite nanofibers is 10 times that for In<sub>2</sub>O<sub>3</sub> nanofibers. In this case, In<sub>2</sub>O<sub>3</sub>, as in mixed systems of nanoparticles, is an electron supplier, while ZnO is a catalytically active agent.

The study of the sensor layer based on core-shell nanofibers was also carried out for the ZnO-SnO<sub>2</sub> system, which has a slightly different crystal structure. These fibers consist of a monocrystal ZnO core and a continuous SnO<sub>2</sub> shell, formed during the thermal reaction of (CH<sub>3</sub>)<sub>4</sub>Sn with oxygen on the ZnO surface [121]. The sensitivity of such a layer to reducing gases (CO, CH<sub>4</sub>, H<sub>2</sub>, C<sub>2</sub>H<sub>5</sub>OH) at 200 and 300 °C is very low and almost does not differ from the sensitivity of a layer of ZnO nanofibers. An increase in the sensor effect, under the influence of the SnO<sub>2</sub> shell located on the surface of ZnO nanofibers, manifests itself only when the temperature rises to 400 °C. Therefore, in ZnO-SnO<sub>2</sub> nanofibers [121], conduction electrons, trapped by defects at the interface between the core and shell, are held more strongly in defects than in the ZnO-SnO<sub>2</sub> and SnO<sub>2</sub>-ZnO nanofibers considered above, with shells formed by the deposition of atomic layers [114,117].

Thus, the sensor properties of composite metal oxide nanofibers of the core-shell type strongly depend on the composition and method of syntheses of the nanofibers (Table 2) and, accordingly, on their morphology. A detailed study of such systems will elucidate the role of the interaction between the core and shell in the sensor process, and will contribute to the development of new, highly efficient sensor materials.

**Table 2.** Sensor responses of core-shell materials to various gases.

Material	Synthesis Method	Sensor Response (Gas Concentration)	Temperature	References
Ag- $\alpha$ -Fe <sub>2</sub> O <sub>3</sub> core-shell composites	two-step reduction-sol gel approach, including Ag nanoparticles	9 (500 ppm)	250 °C	[105]
Au-ZnO core-shell nanoparticles	facile low-temperature solution route	103.9 (100 ppm H <sub>2</sub> )	300 °C	[107]
SnO <sub>2</sub> -ZnO core-shell nanowires	two-step process	25 (10 ppm NO <sub>2</sub> ) 75 (10 ppm C <sub>7</sub> H <sub>8</sub> ) 83 (10 ppm C <sub>6</sub> H <sub>6</sub> ) 77 (10 ppm CO)	300 °C	[108]
SnO <sub>2</sub> -ZnO core-shell nanofibers	two-step process	6.5 (1 ppm CO) 48 (1 ppm NO <sub>2</sub> )	300 °C	[110]
ZnO-CuO core-shell nanowires	facile three-step process	29 (10 ppm NO <sub>2</sub> )	350 °C	[111]
In <sub>2</sub> O <sub>3</sub> /ZnO core-shell nanowires	thermal evaporation of indium powder in an oxidizing atmosphere, followed by the atomic layer deposition of ZnO	196 (1000 ppm C <sub>2</sub> H <sub>5</sub> OH)	300 °C	[113]

Table 2. Cont.

Material	Synthesis Method	Sensor Response (Gas Concentration)	Temperature	References
SnO <sub>2</sub> -ZnO core-shell nanowires functionalized by Au nanoparticles	Vapor-liquid-solid growth method	26.6 (100 ppb CO)	300 °C	[114]
Ag functionalized W <sub>18</sub> O <sub>49</sub> @PPy core-shell nanorods	polymerizing the uniform PPy shell film on surface of W <sub>3</sub> nanorods with AgNO <sub>3</sub> as oxidant and DBSA as modifier.	2.5 (20 ppm NH <sub>3</sub> )	40 °C	[115]
Pd-functionalized SnO <sub>2</sub> -ZnO core-shell nanowires	two-step growth technique. Pd functionalized SnO <sub>2</sub> -ZnO by using the ray radiolysis technique	71 (100 ppb C <sub>6</sub> H <sub>6</sub> )	300 °C	[116]
SnO <sub>2</sub> -ZnO core-shell nanowires functionalized Pt nanoparticles	two-step growth technique. Pt functionalized SnO <sub>2</sub> -ZnO by using the ray radiolysis technique	279 (100 ppb C <sub>7</sub> H <sub>8</sub> )	300 °C	[117]
ZnO-SnO <sub>2</sub> core-shell nanowires	two-step growth technique	41.13 (10 ppm CO) 39.48 (10 ppm C <sub>7</sub> H <sub>8</sub> ) 40.34 (10 ppm C <sub>6</sub> H <sub>6</sub> )	300 °C	[118]
Nb <sub>2</sub> O <sub>5</sub> /ZnO core-shell nanorod	two-step growth process	156 (100 ppm H <sub>2</sub> )	300 °C	[119]
In <sub>2</sub> O <sub>3</sub> -ZnO core-shell nanowires	two-step growth process	265 (400 ppm C <sub>2</sub> H <sub>5</sub> OH) 7 (2000 ppm H <sub>2</sub> )	350 °C	[120]
ZnO-SnO <sub>2</sub> core-shell nanowires	two-step vapor growth method	66.3 (10 ppm NO <sub>2</sub> )	200 °C	[121]

### 3. Modeling of the Electronic Subsystem of Semiconductor Nanoparticles and Properties of Associated Sensitive Layers

The operation mechanism of semiconductor sensors has been described in many studies [10,14,82]. Due to the presence of oxygen vacancies in the oxide nanoparticles that make up the sensitive layer, a noticeable electron density appears in the conduction band. Oxygen molecules from the air are adsorbed on the surface of nanoparticles and dissociate. The resulting oxygen atoms, which are much deeper electron traps than oxygen vacancies, capture electrons from the bulk of the nanoparticles, and the conductivity of the sensitive layer decreases sharply. After the addition of the analyzed gas, its molecules are adsorbed on the surface of the nanoparticles and react with oxygen ions. The captured electrons are subsequently released and returned to the conduction band of the nanoparticle. The conductivity of the sensitive layer increases, constituting the sensor effect.

Many articles have been published on the modeling of the charge distribution in semiconductor nanoparticles and sensor processes. A discussion of these studies, with reference to the numerous assumptions made within them, including erroneous ones, is presented in a review [14]. The most notable of the erroneous assumptions are the use of a flat instead of a real boundary between nanoparticles, the absence of a relationship between the number of oxygen ions on the surface and the electron concentration in the bulk, and the assumption that the density of positively charged donors is constant along the nanoparticle radius, which is true only in the case of fully ionized donors.

In early studies aimed at determining the distribution of electrons in a nanoparticle, it was assumed that positive charges are immobile and, most importantly, that the concentration of electrons in the negatively charged layer on the surface of nanoparticles was chosen arbitrarily. The role of this layer was clearly overestimated.

The nanoparticles that make up the sensitive layers can be conditionally classified into two types, depending on the concentration of conducting electrons. The first type consists of the nanoparticles with a low electron concentration in the conductive zone. Thus, in sensors

based, for example, on  $\text{SnO}_2$ , the concentration of conduction electrons is  $n_c < 10^{16} \text{ cm}^{-3}$ . At a diameter of 100 nm, one such nanoparticle contains no more than one electron, and a negatively charged layer cannot be created. Thus, there is no interference, as a result of shielding electron transfer between nanoparticles.

In another type of nanoparticles at operating temperatures, the sensitive layer contains a sufficiently large number of conduction electrons. In a nanoparticle of the same size (for example,  $\text{In}_2\text{O}_3$ , in which  $n_c \approx 10^{19} - 10^{20} \text{ cm}^{-3}$  [122,123]), the number of electrons can reach  $\sim 10^4 - 10^5$ . Since a significant part of these electrons is captured on the surface of nanoparticles by oxygen atoms, this leads to the appearance, in this case, of a negatively charged layer. Assuming that the nanoparticles are spherical and that the surface is charged uniformly, we use the well-known Gauss theorem, according to which, an electrical charge uniformly distributed on a spherical surface does not create a field inside the sphere. If, on the whole, the nanoparticle is electrically neutral, then the field outside it is also equal to zero.

The electric field inside the nanoparticle is created, due to the uneven distribution of negative and positive charges inside the nanoparticle [31]. The current in the system is determined by the state of electrons in the near-surface layer. To determine the efficiency of the sensor, it is necessary to calculate the distribution of charges over the radius of the nanoparticle, in both the presence and absence of the studied gas. This will make it possible to compare theoretical and experimental results on the sensitivity of sensors based on both single and mixed oxides.

### 3.1. Distribution of Electrons in Oxide Nanoparticles

In sensors based on nanoparticles with a low concentration of conduction electrons (for example,  $\text{SnO}_2$ ), there is no negatively charged layer, the distribution of electrons over the volume is uniform, and there is no problem of finding the charge distribution in the nanoparticle.

For sensors with a high concentration of conduction electrons, the situation is much more complicated. To find the distribution of electrons along the radius of a nanoparticle, one can use the free energy of the system, which consists of the free energies of conduction electrons and electrons on adsorbed oxygen atoms, as well as the potential energy of positively charged ionized donors and the interaction of all negative and positive charges of the nanoparticle [31]. The total free energy is minimized with respect to the chemical potential. Further, the resulting equations are solved, together with a system of stationary equations for the quantity of oxygen atoms, ions, and molecules on the surface of nanoparticles [31,35].

As a result, for nanoparticles of different radii, one can find the distribution of conduction electrons along the nanoparticle radius as a function of temperature. The distribution is found to be inhomogeneous, and the inhomogeneity increases with increasing temperature. This is explained by an increase in the number of electrons on the surface at increasing temperature [37].

### 3.2. Sensor Effect in One-Component Systems

A theory has been constructed that describes the sensor properties of semiconductor oxides containing both small and large quantities of conduction electrons. In the case of one-component sensors, terms and equations for the detected gas are added to the system of stationary kinetic equations for the concentrations of oxygen atoms, ions, and molecules. The solution of this system, together with the equations for the concentration of conduction electrons, makes it possible to find the sensitivity of the sensor as a function of the pressure of the detected gas, the temperature, and the average radius of the nanoparticles [32–35].

The theory developed was compared with the experimental data. For example, in [33] a comparison was made of the theoretical and experimental results obtained in a study on the dependence of sensitivity to different hydrogen concentrations on temperature for sensors with large [124] and small [33] average radii of  $\text{SnO}_2$  nanoparticles. In addition,

the dependence of the sensitivity of a sensor based on tin oxide nanoparticles, on their size, was experimentally studied [125]. It has been shown that the maximum sensitivity of the sensor decreases with an increase in the average size of the nanoparticles. Calculations of the dependences of the sensitivity of the SnO<sub>2</sub> sensor, on temperature and nanoparticle size, showed good agreement with experiment [32,33].

Sensors with a high concentration of conduction electrons have also been studied [34,35]. The technique of determining the electron distribution along the nanoparticle radius has been used for comparing theory with experiment [31]. The electron concentration in the near-surface layer was calculated in the presence and absence of the studied gas. The ratio of these concentrations corresponds to the sensor effect. The study showed a fairly good agreement between the experimental and theoretical results, at reasonable values of the fitting parameters [34,35]. Some discrepancy between theory and experiment is explained by the fact that the calculations were carried out for spherical nanoparticles, which, in fact, differ markedly from reality [35]. In addition, the study assumed average particle radius, without consideration for the dispersion of nanoparticles.

### 3.3. Electron Distribution and Sensor Effect in Two-Component Systems

The distribution of particles and the sensor effect are determined by different types of interaction between nanoparticles in two-component semiconductor systems [19,37,39,126]. There are many experimental studies devoted to the sensor properties of mixed oxides (see, for example, reviews [13,14,103]). The influence of one nanoparticle on the electronic structure of another largely determines these properties. A theoretical consideration of the distribution of electrons in a mixed system was carried out for the first time in [37]. The distribution of electrons in In<sub>2</sub>O<sub>3</sub> nanoparticles surrounded by CeO<sub>2</sub> nanoclusters was studied. The interaction of nanoobjects leads to the effective dissociation of O<sub>2</sub> molecules on the surface of CeO<sub>2</sub> nanoclusters [127], followed by the transfer of oxygen atoms to neighboring In<sub>2</sub>O<sub>3</sub> nanoparticles and the capture of electrons from their bulk [126]. It should be noted that in experiments where the CeO<sub>2</sub>-In<sub>2</sub>O<sub>3</sub> sensor system was studied [14,20,103,126,128–130], the result did not give a simple summation of sensor effects on CeO<sub>2</sub> and In<sub>2</sub>O<sub>3</sub> nanoobjects but showed their synergistic interaction.

The experimental and theoretical results on the CeO<sub>2</sub>-In<sub>2</sub>O<sub>3</sub> sensor system were subsequently compared [131]. A nanostructured system, corresponding to the insert in Figure 5, was considered. The distribution of electrons in the mixed nanocomposites [37] can be used to describe the experimental results [126].

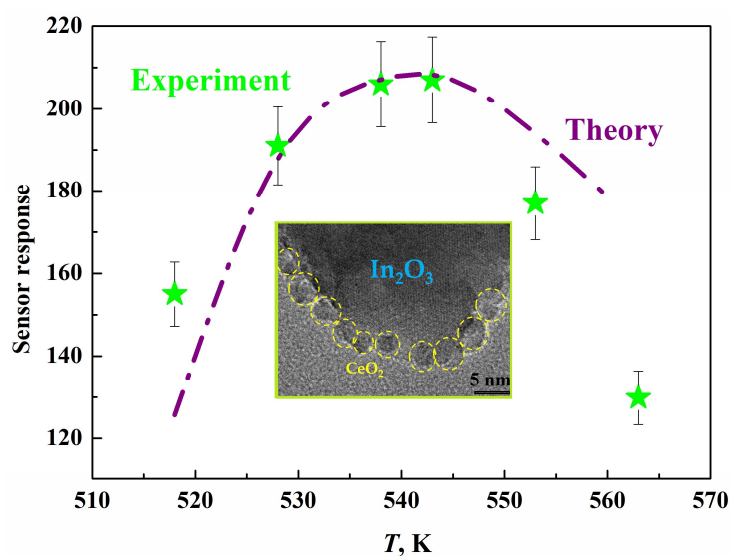


**Figure 5.** Temperature dependence of sensor response of impregnated 3% CeO<sub>2</sub>-97% In<sub>2</sub>O<sub>3</sub> system to hydrogen. Green stars are experimental data [127] and dot-dash line is the theory; the insert is the TEM structure of composite.

Using the mechanism of nanoparticle interaction considered above, it was possible for the first time to describe the temperature dependence of the sensor effect (Figure 5) in a mixed system [132].

#### 4. Mechanisms of Sensor Selectivity

One of the main characteristics of a sensor is the selectivity of its response,  $S_A$ , to the detected chemical compound. In the case of reducing compounds, which are considered in this review, the selectivity is determined mainly by two factors: (i) the selectivity of the adsorption of oxygen molecules and analyzed molecules from air in the near-surface sensor layer, and (ii) the different activity of the adsorbed molecules in the reaction with oxygen anionic centers (mainly  $O^-$ ), capturing the conduction electrons of this semiconductor layer.

At present, there is considerable interest in the detection of harmful anthropogenic substances, the accumulation of which in air is associated with the rapid development of industry [132–134]. The selectivity of the detection of such substances is extremely important for the development of methods for protecting the body from the harmful effects of the external environment.

##### 4.1. Selectivity of Molecule Adsorption on Surface of Sensor Layer

Harmful anthropogenic substances include reducing organic compounds. The reaction of reducing agents with oxygen anion centers on the surface of a semiconductor (mainly metal oxide), which is used for the selective detection of these compounds by the conductometric method. The oxygen anion centers are formed when oxygen molecules capture electrons from the conduction band of the semiconductor.

This process can be conditionally divided into two stages: the adsorption of reagent molecules, and the spillover of the adsorbed molecules from the adsorption center to the oxygen center, accompanied by the reaction of this molecule with the “release” of the trapped electron and its transition to the conduction band of the semiconductor. Such a distinction is valid if the formation of adsorption bonds, between molecules and semiconductor nanoparticles of the sensitive layer of the sensor, does not significantly affect the chemical properties of the molecules, including the reactivity of molecules with respect to the oxygen centers of the sensitive layer.

It is assumed that this feature of adsorption bonds is typical for the interaction of alcohols, aldehydes, and ketones with a metal oxide semiconductor sensor layer. For the selective detection of these compounds, the Brønsted acids are used as nanostructured layers, modified with inclusions of metal oxides with highly basic ions, especially alkali and alkaline earth metal ions. These ions are introduced into the lattice of oxide nanocrystalline particles of the sensitive layer, and form adsorption centers for acid-type compounds. The energy of adsorption bonds, in this case, increases with a decrease in the electronegativity and, consequently, with an increase in the basicity of the introduced ions [135].

The study of nanocrystalline metal oxide layers containing these ions showed that, for such layers, the sensor effect varies, depending on the acidity of adsorbed oxygen-containing compounds, which is determined by their structure. This dependence is the main selectivity factor for the conductometric detection of these compounds by metal oxide sensors [55,57,136].

The use of acid–base bonds, between the analyzed molecules and the nanostructured metal oxide layer, also underlies the selectivity in the detection of compounds related to bases, including amines of various structures [137]. Centers for the selective adsorption of compounds with acidic and basic properties can appear in composites as a result of the mutual charging of molecules during the transfer of electrons between metal ions with different work functions [138,139]. The data obtained indicate a correlation between the acid–base bonds of the detected molecules and the sensitive layer, as well as the magnitude of the sensor effect.

The composite sensitive layers of sensors are considered to contain particles that provide preferential adsorption of molecules of a certain type, with semiconductor particles that form conduction paths. The increase in conductivity in this case, as noted above, is due to the spillover of adsorbed molecules onto the conducting semiconductor layer, where they react with oxygen anionic centers, which gives a selective sensor response.

Further application of this approach to the formation of selective conductometric sensors, by combining adsorbing and conductive components in the sensitive layer, was carried out in [140], where modifiers adsorbing analyzed compounds were grafted onto conductive SnO<sub>2</sub> nanoparticles. Long-chain acid molecules with functional groups were chosen as such modifiers [140]. This method was used to obtain sensors that make it possible to distinguish hydrocarbons, in particular, methane, benzene, and toluene, by the magnitude of the sensor response.

Many harmful anthropogenic substances are present in the atmosphere that belong to various  $\pi$ -electronic compounds, in particular, benzene derivatives. The greatest interest, in the high selectivity detection of these compounds, is on nanostructured metal oxide layers containing transition metal inclusions with partially filled d-electron orbitals.

Adsorption bonds between  $\pi$ -electron molecules and nanoparticles of noble transition metals, in particular, Au, Pd, and Pt, are mainly due to the overlap of the  $\pi$ -electron orbitals of the molecules with the orbitals of the d-electron band of the metal [90]. These bonds depend on the position of the  $\pi$ -electron levels, relative to the center of the d-electron band. It is precisely the formation of these bonds with the subsequent spillover of adsorbed molecules, onto conducting metal oxide nanofibers, that ensures the sensitization of the sensor effect in the composite of nanofibers with noble metal nanoparticles [91].

The dependence of the sensor effect on the energy level of the d-electron band of a metal makes it possible to achieve a high selectivity of the sensor response, by using metal particles with different levels and widths of this band, and also considering the levels of  $\pi$ -electron orbitals of the detected molecules [91,141]. Indeed, doping SnO<sub>2</sub> with Pd, Pt, or Au nanoparticles makes it possible to selectively determine the concentration in air of even sub-ppm amounts of C<sub>6</sub>H<sub>6</sub>, C<sub>7</sub>H<sub>8</sub>, or CO, respectively.

The selectivity observed in these systems is due to the chemical sensitization of the sensor process due to different interactions between the catalytically active metals and the analyzed gas. Thus, the sensor response of Pd-SnO<sub>2</sub> to 1 ppm C<sub>6</sub>H<sub>6</sub> at 300 °C is 25.5, which is almost an order of magnitude higher than the response to C<sub>7</sub>H<sub>8</sub>, C<sub>2</sub>H<sub>5</sub>OH, CO, and H<sub>2</sub>S. On the other hand, SnO<sub>2</sub> composites with Pt or Au have the maximum response to 1 ppm CO (21.1) and C<sub>7</sub>H<sub>8</sub> (40), which also significantly exceeds the response to other gases investigated.

It is important to note that the electronic structure of the surface layer of metal nanoparticles, and the parameters of the d-electron band of this layer, can change due to ligands bound to nanoparticles and deformations of nanoparticles [142]. This opens new possibilities for obtaining selective sensors using noble metal nanoparticles.

#### 4.2. Selective Activity of Adsorbed Molecules in Reaction with Oxygen Anions

In composite metal oxide layers containing clusters of noble metals, the adsorption of detected molecules, especially molecules with  $\pi$ -electron bonds, occurs mainly on these clusters, which have an increased affinity to such molecules. The next stages are the spillover of adsorbed molecules onto the conducting layer of semiconductor metal oxide particles, and the reaction of these molecules with chemisorbed oxygen atoms or molecules that “captured” electrons from the conduction band of the semiconductor. This reaction is accompanied by the return of the “liberated” electrons to the conduction band and, consequently, an increase in the conductivity of the sensor.

However, such a scheme is doubtful at a high bonding energy, between an adsorbed molecule and a metal cluster. For example, the adsorption energy of benzene on a platinum cluster is over 30 kcal/mol and, at the same time, this system has a particularly high sensor response and an extremely short response time [91].

It should be noted that complexes of noble metal clusters, with metal oxide semiconductor nanoparticles in air, already contain chemisorbed oxygen, and this can drastically change the pattern of the sensor process. Most likely, the detected molecule is adsorbed on the complex of the catalytically active metal cluster, with the metal oxide and the negatively charged oxygen center of the sensor reaction, for example,  $O^-$ .

Using the example of a CO molecule adsorbed on such a complex, it has been shown that the adsorption of molecules “triggers” the reaction of CO oxidation and the rearrangement of the initial complex [143]. The reaction,  $CO + O^- \rightarrow CO_2 + e^-$ , produces a sensor response, i.e., leads to an increase in conductivity. Thus, in contrast to the two-stage process considered above, in this case, both adsorption and reaction merge into one reaction.

A sensor process of this type is observed at the interaction of reducing compounds with oxygen centers of nanocomposites consisting of *n*- and *p*-nanoparticles. Sensor characteristics of the *n-p*-nanocomposite depend on the interaction between the particles of its components. In *p-n*-composite semiconductor systems, in which potential barriers at the boundaries of *n*- and *p*-composite nanoparticles prevent the recombination of electrons and holes between particles, the sensor effects depend on the electronic and hole conductivity of the composite. The resulting current flowing through the composite is a combination of the electron current in the conduction band of the composite particles (electron current), and the current, due to electron hopping between positively charged holes in the valence band, in the direction of the electric field (hole current). This situation arises when conducting paths consisting of *n*- and *p*-nanoparticles [23] are simultaneously present in the composite.

In the *p-n*-nanocomposite, when reducing compounds react with oxygen centers on the surface of nanoparticles that have captured conduction electrons, the concentration of these electrons in the particles increases. This leads to an increase in the electronic conductivity ( $\Delta I_e$ ) in the paths consisting of the *n*-type nanoparticles. In *p*-type particles, due to the recombination of positively charged holes with electrons released during the reaction on the surface of these particles, the hole concentration decreases and the hole conductivity ( $\Delta I_h$ ) decreases. As a result, the increase in overall conductivity of a nanostructured *n-p*-composite sensor, upon reaction with a reducing gas (i.e., sensor response), should be less than in a nanostructured sensor consisting only of *n*-nanoparticles. This is confirmed by the data of some studies [24,144].

The sensor response of a nanocomposite *p-n* sensor to reducing compounds depends, firstly, on the adsorption of the detected molecules on the nanoparticles of the sensor's sensitive layer. The difference in the adsorption of detected gases on *n*- and *p*-nanoparticles of this layer significantly increases the selectivity of gas detection.

In particular, the use of a nanostructured *n-SnO<sub>2</sub>-p-Co<sub>3</sub>O<sub>4</sub>* composite sensor made it possible to achieve exceptionally high selectivity in the detection of hydrogen in a mixture with carbon monoxide [24]. This became possible due to different adsorption of H<sub>2</sub> and CO on the *n*- and *p*-nanoparticles of the composite. H<sub>2</sub> is adsorbed and reacts with adsorbed oxygen mainly on the *n-SnO<sub>2</sub>* nanoparticles, while CO is equally adsorbed on the *n-SnO<sub>2</sub>* and *p-Co<sub>3</sub>O<sub>4</sub>* nanoparticles [24]. This means that the decrease in the conductivity considered above, and the decrease in the sensor response of the *n-SnO<sub>2</sub>-p-Co<sub>3</sub>O<sub>4</sub>* composite with an increase in the content of the *p*-hole component (*p-Co<sub>3</sub>O<sub>4</sub>*) in it, will be greater for the detection of CO than the detection of H<sub>2</sub>. Accordingly, the difference between sensor responses to H<sub>2</sub> and CO will increase.

At a certain concentration of Co<sub>3</sub>O<sub>4</sub>, near the percolation transition from the electronic conductivity of the composite to the hole conductivity (in the system [24], at a Co<sub>3</sub>O<sub>4</sub> content of about 15%), the fraction of the conductivity of the “hole” component of Co<sub>3</sub>O<sub>4</sub>, in the total conductivity of the composite, becomes so small that the sensor response of the composite almost does not differ from the response to hydrogen for SnO<sub>2</sub> [24].

High selectivity in the detection of H<sub>2</sub> and CO, in a mixture of these gases, was also found for nanocomposite sensors, *n-SnO<sub>2</sub>-p-Mn<sub>3</sub>O<sub>4</sub>* [144] and *n-ZnO-p-NiO* [145], where the selectivity has the same characteristics as in composites considered in [24]. It was also shown that the annealing temperature of the intermediate mixture of oxides, during the

formation of composites, affects the temperature of electron-hole transitions and sensor responses to CO and H<sub>2</sub> [145]. The observed influence of the annealing temperature on the response opens up new possibilities for controlling the sensor process.

The above results have shown that the doping of sensors based on n-type metal oxides with catalytically active additives leads to the production of sensor materials with high selectivity in the detection of various gases (see Table 3). The influence of the sensor composition on selectivity is due to the electronic and chemical sensitization of the sensor process that occurs during the interaction of the sensitive layer with the analyzed gas.

**Table 3.** Selectivity of various sensor systems in the detection of various chemical compounds.

Material	Synthesis	Gas Selectivity	Temperature	References
ZnO/NiO	ZnO nanorods by the one-pot chemical method, NiO by hydrothermal method	H <sub>2</sub> > CO, NO <sub>2</sub> , CO <sub>2</sub> , CH <sub>4</sub>	237 °C	[145]
Pd-ZnO/NiO	Pd by chemical reduction method, ZnO nanorods by the one-pot chemical method, NiO by hydrothermal method	H <sub>2</sub> > CO, NO <sub>2</sub> , CO <sub>2</sub> , CH <sub>4</sub>	225 °C	[145]
SnO <sub>2</sub> -Mn <sub>3</sub> O <sub>4</sub>	sol-gel technique	H <sub>2</sub> > CO	350 °C	[144]
SnO <sub>2</sub> /Co <sub>3</sub> O <sub>4</sub>	sol-gel technique	H <sub>2</sub> > CO	350 °C	[24]
SnO <sub>2</sub> -ZnO	precipitation method	C <sub>2</sub> H <sub>5</sub> OH > CO	300 °C	[139]
SnO <sub>2</sub>	precipitation method	CO > C <sub>2</sub> H <sub>5</sub> OH	250–300 °C	[139]
SnO <sub>2</sub> -ZnO	hydrothermal method	Trimethylamine > other gases	330 °C	[138]
Nb-doped TiO <sub>2</sub> nanotubes	anodic oxidation method	Dimethylamine > NH <sub>3</sub> , C <sub>2</sub> H <sub>5</sub> OH, CO	300 °C	[137]
5% Ca-In <sub>2</sub> O <sub>3</sub>	electrospun method	Formaldehyde > other volatile organic compounds	130 °C	[136]
5Y-In <sub>2</sub> O <sub>3</sub>	electrospun method	formaldehyde > other gases	100–120 °C	[135]
NiO/ZnO	one-step hydrothermal method	formaldehyde > other volatile organic compounds	200 °C	[134]

## 5. Conclusions

The influence of the interaction of nanoparticles on the sensitivity and selectivity of semiconductor sensors in the detection of reducing gases is considered and analyzed. The primary focus is on various detection mechanisms in two-component metal oxide systems. The mechanisms discussed include the influence of doping on the lattice structure, the adsorption of detected gases, the reactivity of oxygen centers, and various possibilities for sensitization of the sensor process. The role of conduction pathways is also considered.

Particular attention is paid to a direction that has been intensively developing recently—sensors based on core-shell nanofibers. The reasons for the high sensitivity and selectivity of such materials are discussed in sufficient detail. In addition, the possibilities of a theoretical description of the electronic structure of nanoparticles and the sensor process in one-component and two-component systems are briefly considered.

One of the important issues considered in this review is the problem of selectivity. Among the various ways to achieve greater selectivity, this review is limited to the consideration of such mechanisms as the selectivity of the process of adsorption of molecules on the sensitive layer surface, and the selectivity of the reaction of oxygen anions with adsorbed molecules.

It is interesting that different authors note both an increase and a decrease in the sensor effect during doping. The sensitivity of sensors is known to be determined by the ratio of the density of conduction electrons in the surface layers of nanoparticles,

in the presence and absence of the detected gas ( $n_s(P)/n_s(0)$ , where P is the pressure of the detected gas). Sensitivity can be increased either by increasing the numerator or decreasing the denominator. Obviously, at high concentrations of the detected gas, it is better to use nanoparticles with large  $n_s$  to enhance the numerator, while at low concentrations,  $n_s$  should be small, in order to affect the denominator. In other words, for sensors designed to determine the concentrations of toxic and explosive substances close to the MPC (maximum permissible concentrations), it is preferable to use semiconductors with a high concentration of conduction electrons.

The efficiency of the sensor is determined by the following characteristics: sensitivity, sensor response time and relaxation, optimal operating temperature and selectivity. The values achieved for the first three characteristics can be considered quite satisfactory, especially considering the results of operando mode. The situation is more complicated for temperature and selectivity.

Almost all conductometric gas sensors operate at high temperatures (300–500 °C).

Such high temperatures limit the scope of the application of gas sensors, including the impossibility of their integration into mobile devices, as well as the significant power consumption requirement and risk of explosion. Some reduction in operating temperature has been achieved by using mixed nanocomposites, such as the sensitive layer. In the last decade, studies on the photoactivation of detection at room temperatures have been reported, but the efficiency and response/recovery time of such sensors leave much to be desired. The same can be said about the metal-containing sensitive layers synthesized by low-temperature, solid-phase polymerization.

Although the situation with the selectivity of sensors remains unsatisfactory, new opportunities have been opened for solving this problem. The use of composites based on noble metal nanoparticles, for example, is promising in this regard. Moreover, the sensor effect of nanocrystalline metal oxides containing alkali and alkaline-earth metal ions varies depending on the acidity of adsorbed oxygen-containing compounds. This is the main factor for the selective detection of such compounds. Nevertheless, further research is needed to better address this issue.

Another area that needs to be developed is the theoretical study of the structure of semiconductor nanoparticles and the mechanisms of the sensor effect. This is especially important for two-component sensitive layers, because single-component systems have already been widely explored.

**Author Contributions:** Conceptualization, writing—introduction and conclusions, L.I.T.; preparation and visualization, M.I.I.; review and editing, O.J.I.; methodology, V.F.G.; writing—original draft, G.N.G. All authors have read and agreed to the published version of the manuscript.

**Funding:** The work was supported by a subsidy from the Ministry of Education and Science of the RF for N.N. Semenov Federal Research Centre of Chemical Physics, RAS, within the framework of State Assignment No. 122040500071-0.

**Institutional Review Board Statement:** Not applicable.

**Informed Consent Statement:** Not applicable.

**Data Availability Statement:** Not applicable.

**Conflicts of Interest:** The authors declare no conflict of interest.

## References

1. Degler, D.; Weimar, U.; Barsan, N. Current understanding of the fundamental mechanisms of doped and loaded semiconducting metal-oxide-based gas sensing materials. *ACS Sens.* **2019**, *4*, 2228–2249. [[CrossRef](#)] [[PubMed](#)]
2. Degler, D. Trends and advances in the characterization of gas sensing materials based on semiconducting oxides. *Sensors* **2018**, *18*, 3544. [[CrossRef](#)] [[PubMed](#)]
3. Miller, D.R.; Akbar, S.A.; Morris, P.A. Nanoscale metal oxide-based heterojunctions for gas sensing: A review. *Sens. Actuators B* **2014**, *204*, 250–272. [[CrossRef](#)]
4. Barsan, N.; Koziej, D.; Weimar, U. Metal oxide-based gas sensor research: How to? *Sens. Actuators B* **2007**, *121*, 18–35. [[CrossRef](#)]

5. Yamazoe, N.; Sakai, G.; Shimano, K. Oxide semiconductor gas sensors. *Catal. Surv. Asia* **2003**, *7*, 63–75. [CrossRef]
6. Liu, J.; Liu, X.; Zhai, Z.; Jin, G.; Jiang, Q.; Zhao, Y.; Luo, C.; Quan, L. Evaluation of depletion layer width and gas-sensing properties of antimony-doped tin oxide thin film sensors. *Sens. Actuators B* **2015**, *220*, 1354–1360. [CrossRef]
7. Sharma, A.; Rout, C.S. Advances in understanding the gas sensing mechanisms by in situ and operando spectroscopy. *J. Mater. Chem. A* **2021**, *9*, 18175–18207. [CrossRef]
8. Gurlo, A.; Riedel, R. In situ and operando spectroscopy for assessing mechanisms of gas sensing. *Ang. Chem. Intern. Ed.* **2007**, *46*, 3826–3848. [CrossRef]
9. Morrison, S.R. *The Chemical Physics of Surfaces*; Springer Science & Business Media: New York, NY, USA, 2013. Available online: [https://scholar.google.com/scholar\\_lookup?title=The%20Chemical%20Physics%20of%20Surfaces&publication\\_year=1990&author=S.R.%20Morrison](https://scholar.google.com/scholar_lookup?title=The%20Chemical%20Physics%20of%20Surfaces&publication_year=1990&author=S.R.%20Morrison) (accessed on 1 January 2020).
10. Barsan, N.; Weimar, U. Conduction model of metal oxide gas sensors. *J. Electroceramics* **2001**, *7*, 143–167. [CrossRef]
11. Sopiha, K.V.; Malyi, O.I.; Persson, C.; Wu, P. Chemistry of oxygen ionosorption on SnO<sub>2</sub> surfaces. *Appl. Mater. Interfaces* **2021**, *13*, 33664–33676. [CrossRef]
12. Yamazoe, N.; Suematsu, K.; Shimano, K. Extension of receptor function theory to include two types of adsorbed oxygen for oxide semiconductor gas sensors. *Sens. Actuators B* **2012**, *163*, 128–135. [CrossRef]
13. Yamazoe, N.; Kurorawa, Y.; Seiyama, T. Effects of additives on semiconductor gas sensors. *Sens. Actuators B* **1983**, *4*, 283–289. [CrossRef]
14. Gerasimov, G.N.; Gromov, V.F.; Ilegbusi, O.J.; Trakhtenberg, L.I. The mechanisms of sensory phenomena in binary metal-oxide nanocomposites. *Sens. Actuators B* **2017**, *240*, 613–624. [CrossRef]
15. Korotcenkov, G.; Cho, B.K. Instability of metal oxide-based conductometric gas sensors and approaches to stability improvement (short survey). *Sens. Actuators B* **2011**, *156*, 527–538. [CrossRef]
16. Schwarz, A.; Contescu, C.; Contescu, A. Methods for preparation of catalytic materials. *Chem. Rev.* **1995**, *95*, 477–510. [CrossRef]
17. Korotcenkov, G.I.; Cornet, B.; Cirera, J.R.; Golovanov, V.; Boris, I.; Lychkovsky, V.; Karkotsry, Y.; Rodriguez, A. The influence of additives on gas sensing and structural properties of In<sub>2</sub>O<sub>3</sub>-based ceramics. *Sens. Actuators B Chem.* **2007**, *120*, 657–664. [CrossRef]
18. Lin, C.-Y.; Fang, Y.-Y.; Lin, C.-W.; Tunney, J.J.; Ho, K.-C. Fabrication of NO<sub>x</sub> gas sensors using In<sub>2</sub>O<sub>3</sub>-ZnO composite films. *Sens. Actuators B* **2010**, *146*, 28–34. [CrossRef]
19. Gerasimov, G.N.; Ikim, M.I.; Gromov, V.F.; Ilegbusi, O.J.; Trakhtenberg, L.I. Chemical modification of impregnated SnO<sub>2</sub>-In<sub>2</sub>O<sub>3</sub> nanocomposites due to interaction of sensor components. *J. Alloys Compd.* **2021**, *883*, 160817. [CrossRef]
20. Trakhtenberg, L.I.; Gerasimov, G.N.; Gromov, V.F.; Belysheva, T.V.; Ilegbusi, O.J. Effect of composition and temperature on conductive and sensing properties of CeO<sub>2</sub> + In<sub>2</sub>O<sub>3</sub> nanocomposite films. *Sens. Actuators B* **2015**, *209*, 562–569. [CrossRef]
21. Trakhtenberg, L.I.; Gerasimov, G.N.; Gromov, V.F.; Belysheva, T.V.; Ilegbusi, O.J. Effect of composition on sensing properties of SnO<sub>2</sub> + In<sub>2</sub>O<sub>3</sub> mixed nanostructured films. *Sens. Actuators B* **2012**, *169*, 32–38. [CrossRef]
22. Trakhtenberg, L.I.; Gerasimov, G.N.; Gromov, V.F.; Belysheva, T.V.; Ilegbusi, O.J. Conductivity and sensing properties of In<sub>2</sub>O<sub>3</sub> + ZnO mixed nanostructured films: Effect of composition and temperature. *Sens. Actuators B* **2013**, *187*, 514–521. [CrossRef]
23. Kim, J.-H.; Lee, J.-H.; Mirzaei, A.; Kim, H.W.; Kim, S.S. Optimization and gas sensing mechanism of *n*-SnO<sub>2</sub>-*p*-Co<sub>3</sub>O<sub>4</sub> composite nanofibers. *Sens. Actuators B* **2017**, *248*, 500–511. [CrossRef]
24. Yin, X.-T.; Li, J.; Dastan, D.; Zhou, W.-D.; Garmestani, H.; Alamgir, F.M. Ultra-high selectivity of H<sub>2</sub> over CO with a *p-n* nanojunction based gas sensors and its mechanism. *Sens. Actuators B* **2020**, *319*, 128330. [CrossRef]
25. Yamazoe, N. New approaches for improving semiconductor gas sensors. *Sens. Actuators B* **1991**, *5*, 7–19. [CrossRef]
26. Yamazoe, N.; Shimano, K. Receptor function and response of semiconductor gas sensor. *J. Sens.* **2009**, *138*, 875704. [CrossRef]
27. Nagaev, E.L. Small metal particles. *Soviet Phys. Uspekhi* **1992**, *35*, 747–782. [CrossRef]
28. Trakhtenberg, L.I.; Gerasimov, G.N.; Grigoriev, E.I.; Zavialov, S.A.; Zagorskaja, O.V.; Zufman, V.Y.; Smirnov, V.V. Nanoheterogeneous metal-polymer composites as a new type of effective and selective catalysts. *Stud. Surf. Sci. Catal.* **2000**, *130*, 941–946. [CrossRef]
29. Maier, J.; Göpel, W. Investigations of the bulk defect chemistry of polycrystalline tin (IV) oxide. *J. Solid State Chem.* **1988**, *72*, 293–302. [CrossRef]
30. Kolmakov, A.; Klenov, D.O.; Lilach, Y.; Stemmer, S.; Moskovits, M. Enhanced gas sensing by individual SnO<sub>2</sub> nanowires and nanobelts functionalized with Pd catalyst particles. *Nano Lett.* **2005**, *5*, 667–673. [CrossRef]
31. Kozhushner, M.A.; Lidskii, B.V.; Oleynik, I.I.; Posvyanskii, V.S.; Trakhtenberg, L.I. Inhomogeneous charge distribution in semiconductor nanoparticles. *J. Phys. Chem. C* **2015**, *119*, 16286–16292. [CrossRef]
32. Kozhushner, M.A.; Trakhtenberg, L.I.; Landerville, A.C.; Oleynik, I.I. Theory of sensing response of nanostructured tin-dioxide thin films to reducing hydrogen gas. *J. Phys. Chem. C* **2013**, *117*, 11562–11568. [CrossRef]
33. Kozhushner, M.A.; Trakhtenberg, L.I.; Bodneva, V.L.; Belysheva, T.V.; Landerville, A.C.; Oleynik, I.I. Effect of temperature and nanoparticle size on sensor properties of nanostructured tin dioxide films. *J. Phys. Chem. C* **2014**, *118*, 11440–11444. [CrossRef]
34. Kozhushner, M.A.; Bodneva, V.L.; Oleynik, I.I.; Belysheva, T.V.; Ikim, M.I.; Trakhtenberg, L.I. Sensor effect in oxide films with a large concentration of conduction electrons. *J. Phys. Chem. C* **2017**, *121*, 6940–6945. [CrossRef]
35. Bodneva, V.L.; Ilegbusi, O.J.; Kozhushner, M.A.; Kurmangaleev, K.S.; Posvyanskii, V.S.; Trakhtenberg, L.I. Modeling of sensor properties for reducing gases and charge distribution in nanostructured oxides: A comparison of theory with experimental data. *Sens. Actuators B* **2019**, *287*, 218–224. [CrossRef]

36. Trakhtenberg, L.I.; Ilegbusi, O.J.; Kozhushner, M.A. Calculation of the electric potential and surface oxygen ion density for planar and spherical metal oxide grains by numerical solution of the Poisson equation coupled with Boltzmann and Fermi-Dirac statistics. *Sens. Actuators B Chem.* **2019**, *293*, 31–40, Comment in *Sens. Actuators B* **2020**, *302*, 126986. [[CrossRef](#)]
37. Kurmangaleev, K.S.; Ikim, M.I.; Kozhushner, M.A.; Trakhtenberg, L.I. Electron distribution and electrical resistance in nanostructured mixed oxides CeO<sub>2</sub>-In<sub>2</sub>O. *Appl. Surf. Sci.* **2020**, *546*, 149011. [[CrossRef](#)]
38. Aragon, F.H.; Coaquira, J.A.H.; Hidalgo, P.; daSilva, S.W.; Brito, S.L.M.; Gouvêa, D.; Morais, P.C. Evidences of the evolution from solid solution to surface segregation in Ni-doped SnO<sub>2</sub> nanoparticles using Raman spectroscopy. *J. Raman Spectrosc.* **2011**, *42*, 1081–1086. [[CrossRef](#)]
39. Luo, Y.; An, B.; Bai, J.; Wang, Y.; Cheng, X.; Wang, Q.; Li, J.; Yang, Y.; Wu, Z.; Xie, E. Ultrahigh-response hydrogen sensor based on PdO/NiO co-doped In<sub>2</sub>O<sub>3</sub> nanotubes. *J. Colloid Interface Sci.* **2021**, *599*, 533–542. [[CrossRef](#)]
40. Gerasimov, G.N.; Gromov, V.F.; Ikim, M.I.; Ilegbusi, O.J.; Ozerin, S.A.; Trakhtenberg, L.I. Structure and gas-sensing properties of SnO<sub>2</sub>-In<sub>2</sub>O<sub>3</sub> nanocomposites synthesized by impregnation method. *Sens. Actuators B* **2020**, *320*, 128406. [[CrossRef](#)]
41. Zhu, X.; Li, Y.; Zhang, H.; Song, L.; Zu, H.; Qin, Y.; Liu, L.; Li, Y.; Wang, F. High-performance field effect transistors based on large ratio metal (Al, Ga, Cr) doped In<sub>2</sub>O<sub>3</sub> nanofibers. *J. Alloys Compd.* **2020**, *830*, 154578. [[CrossRef](#)]
42. Sakthiraj, K.; Balachandrakumar, K. Influence of Ti addition on the room temperature ferromagnetism of tin oxide (SnO<sub>2</sub>) nanocrystal. *J. Magn. Mater.* **2015**, *395*, 205–212. [[CrossRef](#)]
43. Shen, J.; Li, F.; Yin, B.; Sun, L.; Chen, C.; Wen, S.; Chen, Y.; Ruan, S. Enhanced ethyl acetate sensing performance of Al-doped In<sub>2</sub>O<sub>3</sub> microcubes. *Sens. Actuators B* **2017**, *253*, 461–469. [[CrossRef](#)]
44. Al-Hashem, M.; Akbar, S.; Morris, P. Role of oxygen vacancies in nanostructured metal-oxide gas sensors: A review. *Sens. Actuators B* **2019**, *301*, 126845. [[CrossRef](#)]
45. Zeng, X.; Liu, L.; Lv, Y.; Zhao, B.; Ju, X.; Xu, S.; Zhang, J.; Tian, C.; Sun, D.; Tang, X. Ultra-sensitive and fast response formaldehyde sensor based on La<sub>2</sub>O<sub>3</sub>-In<sub>2</sub>O<sub>3</sub> beaded na-notubes at low temperature. *Chem. Phys. Lett.* **2020**, *746*, 137289. [[CrossRef](#)]
46. Lemos, S.C.S.; Nossol, E.; Ferrari, J.L.; Gomes, E.O.; Andres, J.; Gracia, L.; Sorribes, I.; Lima, R.C. Joint theoretical and experimental study on the la doping process in In<sub>2</sub>O<sub>3</sub>: Phase transition and electrocatalytic activity. *Inorg. Chem.* **2019**, *58*, 11738. [[CrossRef](#)]
47. Aragon, F.H.; Coaquira, J.A.H.; Villegas-Lelovsky, L.; da Silva, S.W.; Cesar, D.F.; Nagamine, L.C.C.M.; Cohen, R.; Men'endez-Proupin, E.; Morais, P.C. Evolution of the doping regimes in the Al-doped SnO<sub>2</sub> nanoparticles prepared by a polymer precursor method. *J. Phys. Condens. Matter* **2015**, *27*, 095301. [[CrossRef](#)]
48. An, Y.; Yang, D.; Ma, G.; Zhu, Y.; Wang, S.; Wu, Z.; Liu, J. Role of Co cluster and oxygen vacancies in the magnetic and transport properties of Co-doped In<sub>2</sub>O<sub>3</sub> films. *J. Phys. Chem. C* **2014**, *118*, 10448–10454. [[CrossRef](#)]
49. Liu, X.; Zhang, S.; Wu, Z.; An, Y. Manganese-vacancy complexes induced room temperature ferromagnetism in Mn/Mg co-doped In<sub>2</sub>O<sub>3</sub> diluted magnetic semiconductors. *Superlattices Microstruct.* **2019**, *132*, 106174. [[CrossRef](#)]
50. Yamaura, H.; Moriya, K.; Miura, N.; Yamazoe, N. Mechanism of sensitivity promotion in CO sensor using indium oxide and cobalt oxide. *Sens. Actuators B* **2000**, *65*, 39–41. [[CrossRef](#)]
51. Bloch, E.D.; Hudson, M.R.; Mason, J.A.; Chavan, S.; Crocellà, V.; Howe, J.D.; Lee, K.; Dzubak, A.L.; Queen, J.W.L.; Zadrozny, M.; et al. Reversible CO binding enables tunable CO/H<sub>2</sub> and CO/N<sub>2</sub> separations in metal-organic frameworks with exposed divalent metal cations. *J. Am. Chem. Soc.* **2014**, *136*, 10752–10761. [[CrossRef](#)]
52. Jinkawa, T.; Sakai, G.; Tamaki, J.; Miura, N.; Yamazoe, N. Relationship between ethanol gas sensitivity and surface catalytic property of tin oxide sensors modified with acidic or basic oxides. *J. Mol. Catal. A* **2000**, *155*, 193–200. [[CrossRef](#)]
53. Lupinetti, A.J.; Fau, S.; Frenking, G.; Strauss, S.H. Theoretical analysis of the bonding between CO and positively charged atoms. *J. Phys. Chem. A* **1997**, *101*, 9551–9559. [[CrossRef](#)]
54. Hocking, R.K.; Hambley, T.W. Database analysis of transition metal carbonyl bond lengths: Insight into the periodicity of  $\pi$  back-bonding,  $\sigma$  donation, and the factors affecting the electronic structure of the TM-CtO moiety. *Organometallics* **2007**, *26*, 2815–2823. [[CrossRef](#)]
55. Liang, Q.; Zou, X.; Chen, H.; Fan, M.; Dong, G.-L. High-performance formaldehyde sensing realized by alkaline-earth metals doped In<sub>2</sub>O<sub>3</sub> nanotubes with optimized surface properties. *Sens. Actuators B* **2020**, *304*, 127241–127246. [[CrossRef](#)]
56. Gao, L.; Fu, H.; Zhu, J.; Wang, J.; Chen, Y.; Liu, H. Synthesis of SnO<sub>2</sub> nanoparticles for formaldehyde detection with high sensitivity and good selectivity. *J. Mater. Res.* **2020**, *35*, 2208–2217. [[CrossRef](#)]
57. Zhao, Y.; Zou, X.; Chen, H.; Chu, X.; Li, G.-D. Tailoring energy level and surface basicity of metal oxide semiconductors by rare-earth incorporation for high-performance formaldehyde detection. *Inorg. Chem. Front.* **2019**, *6*, 1767–1774. [[CrossRef](#)]
58. Dimitrov, V.; Komatsu, T. Correlation among electronegativity, cation polarizability, optical basicity and single bond strength of simple oxides. *J. Solid State Chem.* **2012**, *196*, 574–578. [[CrossRef](#)]
59. Mahajan, S.; Jagtap, S. Metal-oxide semiconductors for carbon monoxide (CO) gas sensing: A review. *Appl. Mater. Today* **2020**, *18*, 100483. [[CrossRef](#)]
60. Hurlburt, P.K.; Rack, J.J.; Luck, J.S.; Dec, S.F.; Webb, J.D.; Anderson, O.P.; Strauss, S.H. Nonclassical metal carbonyls: [Ag(CO)]<sup>+</sup> and [Ag(CO)<sub>2</sub>]<sup>+</sup>. *J. Am. Chem. Soc.* **1994**, *116*, 10003–10014. [[CrossRef](#)]
61. Kim, S.-J.; Hwang, I.-S.; Kang, Y.C.; Lee, J.-H. Design of selective gas sensors using additive-loaded In<sub>2</sub>O<sub>3</sub> hollow spheres prepared by combinatorial hydrothermal reactions. *Sensors* **2011**, *11*, 10603–10614. [[CrossRef](#)]
62. Singh, N.; Comini, E.; Ponzoni, A.; Lee, P.S. Chemical sensing investigation on Zn-In<sub>2</sub>O<sub>3</sub> nanowires. *Sens. Actuators B* **2012**, *171–172*, 244–248. [[CrossRef](#)]

63. Zhou, Q.; Chen, W.; Xu, L.; Kumar, R.; Gui, Y.; Zhao, Z.; Tang, C.; Zhu, S. Highly sensitive carbon monoxide (CO) gas sensors based on Ni and Zn doped SnO<sub>2</sub> nanomaterials. *Ceram. Int.* **2018**, *44*, 4392–4399. [CrossRef]
64. Chen, H.; Zhao, Y.; Shi, L.; Li, G.-D.; Sun, L.; Zou, X. Revealing the relationship between energy level and gas sensing performance in heteroatom-doped semiconducting nanostructures. *ACS Appl. Mater. Interfaces* **2018**, *10*, 29795–29804. [CrossRef]
65. Chen, H.; Sun, L.; Li, G.-D.; Zou, X. Well-tuned surface oxygen chemistry of cation off-stoichiometric spinel oxides for highly selective and sensitive formaldehyde detection. *Chem. Mater.* **2018**, *30*, 2018–2027. [CrossRef]
66. Wang, Z.; Hou, C.; De, Q.; Gu, F.; Han, D. One-step synthesis of Co-doped In<sub>2</sub>O<sub>3</sub> nanorods for high response of formaldehyde sensor at low temperature. *ACS Sens.* **2018**, *3*, 468–475. [CrossRef]
67. Bonu, V.; Das, A.; Prasad, A.K.; Krishna, N.G.; Dhara, S.; Tyagi, A.K. Influence of in-plane and bridging oxygen vacancies of SnO<sub>2</sub> nanostructures on CH<sub>4</sub> sensing at low operating temperatures. *Appl. Phys. Lett.* **2014**, *105*, 243102. [CrossRef]
68. Liu, L.; Shu, S.; Zhang, G.; Liu, S. Highly selective sensing of C<sub>2</sub>H<sub>6</sub>O, HCHO, and C<sub>3</sub>H<sub>6</sub>O gases by controlling SnO<sub>2</sub> nanoparticle vacancies. *ACS Appl. Nano Mater.* **2018**, *1*, 31–37. [CrossRef]
69. Kumar, R.; Jaiswal, M.; Singh, O.; Gupta, A.; Ansari, M.S.; Mittal, J. Selective and reversible sensing of low concentration of carbon monoxide gas using Nb-doped OMS-2 nanofibers at room temperature. *IEEE Sens. J.* **2019**, *19*, 7201–7206. [CrossRef]
70. Genuino, H.C.; Seraji, M.S.; Meng, Y.; Valencia, D.; Suib, S.L. Combined experimental and computational study of CO oxidation promoted by Nb in manganese oxide octahedral molecular sieves. *Appl. Catal. B Environ.* **2015**, *163*, 361–369. [CrossRef]
71. Kuntaiah, K.; Sudarsanam, P.; Reddy, B.M.; Vinu, A. Nanocrystalline Ce<sub>1-x</sub>Sm<sub>x</sub>O<sub>2-δ</sub> (x = 0.4) solid solutions: Structural characterization versus CO oxidation. *RSC Adv.* **2013**, *3*, 7953–7962. [CrossRef]
72. Savage, N.; Chwieroth, B.; Ginwalla, A.; Patton, B.R.; Akbar, S.A.; Dutta, P.K. Composite *n-p*-semiconducting titanium oxide as gas sensors. *Sens. Actuators B* **2001**, *79*, 17–27. [CrossRef]
73. Efron, A.L. *Physics and Geometry of Disorder: Percolation Theory*; Mir: Moscow, Russia, 1986. Available online: <https://archive.org/details/physics-of-disorder> (accessed on 20 May 2023).
74. Choi, S.-W.; Katoch, A.; Kim, J.-H.; Kim, S.S. Striking sensing improvement of n-type oxide nanowires by electronic sensitization based on work function difference. *J. Mater. Chem. C* **2015**, *3*, 1521–1527. [CrossRef]
75. Nam, B.; Ko, T.-K.; Hyun, S.-K.; Lee, C. NO<sub>2</sub> sensing properties of WO<sub>3</sub>-decorated In<sub>2</sub>O<sub>3</sub> nanorods and In<sub>2</sub>O<sub>3</sub>-decorated WO<sub>3</sub> nanorods. *Nano Converg.* **2019**, *6*, 40. [CrossRef] [PubMed]
76. Dey, A. Semiconductor metal oxide gas sensors: A review. *Mater. Sci. Eng. B* **2018**, *229*, 206–217. [CrossRef]
77. Sowmya, B.; Athira, J.; Panda, P.K. A review on metal-oxide based *p-n* and *n-n* heterostructured nanomaterials for gas sensing applications. *Sens. Int.* **2021**, *2*, 100085. [CrossRef]
78. Mirzaei, A.; Yousefi, H.R.; Falsafi, F.; Bonyani, M.; Lee, J.-H.; Kim, J.-H.; Kim, H.W.; Kim, S.S. An overview on how Pd on resistive-based nanomaterial gas sensors can enhance response toward hydrogen gas. *Int. J. Hydrogen Energy* **2019**, *44*, 20522–20571. [CrossRef]
79. Dhall, S.; Kumar, M.; Bhatnagar, M.; Mehta, B.R. Dual gas sensing properties of graphene-Pd/SnO<sub>2</sub> composites for H<sub>2</sub> and ethanol: Role of nanoparticles-graphene interface. *Int. J. Hydrogen Energy* **2018**, *43*, 17921–17927. [CrossRef]
80. Feng, Q.; Li, X.; Wang, J. Percolation effect of reduced graphene oxide (rGO) on ammonia sensing of rGO-SnO<sub>2</sub> composite based sensor. *Sens. Actuators B* **2017**, *243*, 1115–1126. [CrossRef]
81. Sygellou, L.; Paterakis, G.; Galiotis, C.; Tasis, D. Work function tuning of reduced graphene oxide thin films. *J. Phys. Chem. C* **2016**, *120*, 281–290. [CrossRef]
82. Yamazoe, N.; Shimanoe, K. Theory of power laws for semiconductor gas sensors. *Sens. Actuators B* **2008**, *128*, 566–573. [CrossRef]
83. Li, T.; Zeng, W.; Wang, Z. Quasi-one-dimensional metal-oxide-based heterostructural gas-sensing materials: A review. *Sens. Actuators B* **2015**, *221*, 1570–1585. [CrossRef]
84. Hübner, M.; Simion, C.E.; Tomescu-Stanoi, A.; Pokhrel, S.; Bârsan, N.; Weimar, U. Influence of humidity on CO sensing with *p*-type CuO thick film gas sensors. *Sens. Actuators B* **2011**, *153*, 347–353. [CrossRef]
85. Pokhrel, S.; Simion, C.E.; Quemener, V.; Bârsan, N.; Weimar, U. Investigations of conduction mechanism in Cr<sub>2</sub>O<sub>3</sub> gas sensing thick films by ac impedance spectroscopy and work function changes measurements. *Sens. Actuators B* **2008**, *133*, 78–83. [CrossRef]
86. Kim, J.-H.; Lee, J.-H.; Mirzaei, A.; Kim, H.W.; Kim, S.S. (*n*)-SnO<sub>2</sub>—(*p*)-NiO composite nanowires: Gas sensing properties and sensing mechanisms. *Sens. Actuators B* **2018**, *258*, 204–214. [CrossRef]
87. Zhou, W.; Dastan, D.; Yin, X.; Nie, S.; Wu, S.; Wang, Q.; Li, J. Optimization of gas sensing properties of *n*-SnO<sub>2</sub>/*p*-xCuO sensors for homogenous gases and the sensing mechanism. *J. Mater. Sci. Mater. Electron.* **2020**, *31*, 18412–18426. [CrossRef]
88. Zhang, R.; Cao, S.; Zhou, T.; Fei, T.; Wang, R.; Zhang, T. Rational design and tunable synthesis of Co<sub>3</sub>O<sub>4</sub> nanoparticle-incorporating into In<sub>2</sub>O<sub>3</sub> one-dimensional ribbon as effective sensing material for gas detection. *Sens. Actuators B* **2020**, *10*, 127695. [CrossRef]
89. Korotcenkov, G.; Cho, B.K. Metal oxide composites in conductometric gas sensors: Achievements and challenges. *Sens. Actuators B* **2017**, *244*, 182–210. [CrossRef]
90. Walker, J.M.; Akbar, S.A.; Morris, P.A. Synergistic effects in gas sensing semiconducting oxide nanoheterostructures: A review. *Sens. Actuators B* **2019**, *286*, 624–640. [CrossRef]
91. Kim, J.-H.; Wu, P.; Kim, H.W.; Kim, S.S. Highly selective sensing of CO, C<sub>6</sub>H<sub>6</sub>, and C<sub>7</sub>H<sub>8</sub> gases by catalytic functionalization with metal nanoparticles. *ACS Appl. Mater. Interfaces* **2016**, *8*, 7173–7183. [CrossRef]

92. Gromov, V.F.; Gerasimov, G.N.; Belysheva, T.V.; Ikim, M.I.; Spiridonova, E.Y.; Grekhov, M.M.; Ali-zade, R.A.; Trakhtenberg, L.I. Sensor properties of nanostructured systems based on indium oxide with  $\text{Co}_3\text{O}_4$  or  $\text{ZrO}_2$  additives. *Russ. J. Phys. Chem. B* **2018**, *12*, 129–134. [[CrossRef](#)]
93. Nowotny, J.; Sloma, M.; Weppner, W. Surface reactivity of yttria-doped zirconia with oxygen. *Solid State Ionics* **1989**, *32–33*, 709–713. [[CrossRef](#)]
94. Zakrzewska, K.; Radecka, M.  $\text{TiO}_2$ - $\text{SnO}_2$  composites and solid solutions for chemical nanosensors. *Procedia Eng.* **2012**, *47*, 1077–1083. [[CrossRef](#)]
95. Korotcenkov, G.; Han, S.H.; Cho, B.K. Metal Oxide Nanocomposites: Advantages and shortcomings for application in conductometric gas sensors. *Mater. Sci. Forum* **2016**, *872*, 223–229. [[CrossRef](#)]
96. Xu, H.; Ju, D.; Li, W.; Zhang, J.; Wang, J.; Cao, B. Superior triethylamine-sensing properties based on  $\text{TiO}_2/\text{SnO}_2$  *n-n* heterojunction nanosheets directly grown on ceramic tubes. *Sens. Actuators B* **2016**, *228*, 634–642. [[CrossRef](#)]
97. Zhang, K.; Shen, Y.; Li, Y.; Zhang, W. Synthesis of  $\text{ZnO}/\text{In}_2\text{O}_3$  heterojunction with unique hexagonal three-dimensional structure for ultra sensitive ethanol detection. *Mater. Sci. Semicond. Process.* **2022**, *143*, 106523. [[CrossRef](#)]
98. Li, R.; Zhou, Y.; Sun, M.; Gong, Z.; Guo, Y.; Wu, F.; Li, W.; Ding, W. Influence of charge carriers concentration and mobility on the gas sensing behavior of tin dioxide thin films. *Coatings* **2019**, *9*, 591–597. [[CrossRef](#)]
99. Park, S.; Sun, G.-J.; Kheel, H.; Lee, W.I.; Lee, S.; Choi, S.-B.; Lee, C. Synergistic effects of codecoration of oxide nanoparticles on the gas sensing performance of  $\text{In}_2\text{O}_3$  nanorods. *Sens. Actuators B* **2016**, *227*, 591–599. [[CrossRef](#)]
100. Wei, X.; Xie, T.; Peng, L.; Fu, W.; Chen, J.; Gao, Q.; Hong, G.; Wang, D. Effect of heterojunction on the behavior of photogenerated charges in  $\text{Fe}_3\text{O}_4/\text{Fe}_2\text{O}_3$  nanoparticle photocatalysts. *J. Phys. Chem. C* **2011**, *115*, 8637–8642. [[CrossRef](#)]
101. Feste, P.D.; Crisci, M.; Barbon, F.; Tajoli, F.; Salerno, M.; Drago, F.; Prato, M.; Gross, S.; Gatt, T.; Lamberti, F. Work function tuning in hydrothermally synthesized vanadium-doped  $\text{MoO}_3$  and  $\text{Co}_3\text{O}_4$  mesostructures for energy conversion devices. *Appl. Sci.* **2021**, *11*, 2016. [[CrossRef](#)]
102. Sun, Y.; Zhao, Z.; Suematsu, K.; Zhang, W.; Zhang, W.; Zhuyikov, S.; Shimano, K.; Hu, J. MOF-derived Au-NiO/ $\text{In}_2\text{O}_3$  for selective and fast detection of toluene at ppb-level in high humid environments. *Sens. Actuators B* **2022**, *360*, 13163. [[CrossRef](#)]
103. Mirzaei, A.; Kim, J.-H.; Kim, H.W.; Kim, S.S. How shell thickness affects the gas sensing properties of nanostructured materials: Survey of literature. *Sens. Actuators B* **2018**, *256*, 270–294. [[CrossRef](#)]
104. Wang, S.; Kang, Y.; Wang, L.; Zhang, H.; Wang, Y. Organic/inorganic hybrid sensors: A review. *Sens. Actuators B* **2013**, *182*, 467–482. [[CrossRef](#)]
105. Mirzaei, A.; Janghorban, K.; Hashemi, B.; Neri, G. Synthesis, characterization and gas sensing properties of  $\text{Ag}/\alpha\text{-Fe}_2\text{O}_3$  core-shell nanocomposites. *Nanomaterials* **2015**, *17*, 737–749. [[CrossRef](#)] [[PubMed](#)]
106. Karnati, P.; Akbar, S.; Morris, P.A. Conduction mechanisms in one dimensional core-shell nanostructures for gas sensing; A review. *Sens. Actuators B* **2019**, *295*, 127–143. [[CrossRef](#)]
107. Majhi, P.; Rai, Y.-T. Facile approach to synthesize Au-ZnO core shell nanoparticles and their application for highly sensitive and selective gas sensors. *ACS Appl. Mater. Interfaces* **2015**, *7*, 9462–9468. [[CrossRef](#)]
108. Choi, S.-W.; Katoch, A.; Sun, G.-J.; Kim, J.-H.; Kim, S.-H.; Kim, S.-S. Dual functional sensing mechanism in  $\text{SnO}_2$ -ZnO core-shell nanowires. *ACS Appl. Mater. Interfaces* **2014**, *6*, 8281. [[CrossRef](#)]
109. Lee, D.-J.; Kim, K.-J.; Kim, S.-H.; Kwon, J.-Y.; Xu, J.; Kim, K.-B. Atomic layer deposition of Ti-doped ZnO films with enhanced electron mobility. *J. Mater. Chem. C* **2013**, *1*, 4761. [[CrossRef](#)]
110. Katoch, A.; Choi, S.-W.; Sun, G.-J.; Kim, S.-S. An approach to detecting a reducing gas by radial modulation of electron-depleted shells in core-shell nanofibers. *J. Mater. Chem. A* **2013**, *1*, 13588–13596. [[CrossRef](#)]
111. Diao, K.; Xiao, J.; Zheng, Z.; Cui, X. Enhanced sensing performance and mechanism of CuO nanoparticle-loaded. *Appl. Surf. Sci.* **2018**, *459*, 630–638. [[CrossRef](#)]
112. Barsan, N.; Simion, C.; Heine, T.; Pokhrel, S.; Weimar, U. Modeling of sensing and transduction for *p*-type semiconducting metal oxide based gas sensors. *J. Electroceram.* **2010**, *25*, 11–19. [[CrossRef](#)]
113. Park, S.; Ko, H.; Kim, S.; Lee, C. Role of the interfaces in multiple networked one-dimensional core-shell nanostructured gas sensors. *ACS Appl. Mater. Interfaces* **2014**, *6*, 9595–9600. [[CrossRef](#)] [[PubMed](#)]
114. Kim, J.-H.; Mirzaei, A.; Kim, H.W.; Kim, S.S. Extremely sensitive and selective sub-ppm CO detection by the synergistic effect of Au nanoparticles and core-shell nanowires. *Sens. Actuators B* **2017**, *249*, 177–188. [[CrossRef](#)]
115. Qin, Y.; Wen, Z.; Zhang, T. Facile realization of Ag functionalized  $\text{W}_{18}\text{O}_{49}/\text{PPy}$  core-shell nanorods for multieffect modulation on gas sensing response. *J. Mater. Sci. Mater. Electron.* **2019**, *30*, 15031–15041. [[CrossRef](#)]
116. Kim, J.-H.; Kim, H.W.; Kim, S.S. Ultra-sensitive benzene detection by a novel approach: Core-shell nanowires combined with Pd-functionalization. *Sens. Actuators B* **2017**, *239*, 578–585. [[CrossRef](#)]
117. Kim, J.-H.; Kim, S.S. Realization of ppb-scale toluene-sensing abilities with Pt-functionalized  $\text{SnO}_2$ -ZnO core-shell nanowires. *ACS Appl. Mater. Interfaces* **2015**, *7*, 17199–17208. [[CrossRef](#)] [[PubMed](#)]
118. Kim, J.-H.; Mirzaei, A.; Kim, H.W.; Kim, S.S. Variation of shell thickness in ZnO- $\text{SnO}_2$  core-shell nanowires for optimizing sensing behaviors to CO,  $\text{C}_6\text{H}_6$ , and  $\text{C}_7\text{H}_8$  gases. *Sens. Actuators B* **2020**, *302*, 127150. [[CrossRef](#)]
119. Park, S.; Lee, S.; Kim, H.W.; Lee, C. Hydrogen sensing properties of multiple networked  $\text{Nb}_2\text{O}_5/\text{ZnO}$  core-shell nanorod sensors. *Sens. Actuators B* **2014**, *202*, 840–845. [[CrossRef](#)]

120. Singh, N.; Ponzoni, A.; Gupta, R.K.; Lee, P.S.; Comini, E. Synthesis of In<sub>2</sub>O<sub>3</sub>-ZnO core-shell nanowires and their application in gas sensing. *Sens. Actuators B* **2011**, *160*, 1346–1351. [[CrossRef](#)]
121. Hwang, I.-S.; Kim, S.-J.; Choi, J.-K.; Choi, J.; Ji, H.; Kim, G.-T.; Cao, G.; Lee, J.-H. Synthesis and gas sensing characteristics of highly crystalline ZnO-SnO<sub>2</sub> core-shell nanowires. *Sens. Actuators B* **2010**, *148*, 595–600. [[CrossRef](#)]
122. Jimenez, L.C.; Mendez, H.A.; Paez, B.A.; Ramirez, M.E.; Rodriguez, H. Production and characterization of indium oxide and indium nitride. *Braz. J. Phys.* **2006**, *36*, 1017–1024. [[CrossRef](#)]
123. Prathap, P.; Devi, G.G.; Subbaiah, Y.P.V.; Ramakrishna Reddy, K.T.; Ganesan, V. Growth and characterization of indium oxide films. *Curr. Appl. Phys.* **2008**, *8*, 120–124. [[CrossRef](#)]
124. Ahlers, S.; Miller, G.; Doll, T. A rate equation approach to the gas sensitivity of thin film metal oxide materials. *Sens. Actuators B* **2005**, *107*, 587–599. [[CrossRef](#)]
125. Xu, C.; Tamaki, J.; Miura, N.; Yamazoe, N. Grain size effects on gas sensitivity of porous SnO<sub>2</sub>-based elements. *Sens. Actuators B* **1991**, *3*, 147–155. [[CrossRef](#)]
126. Gerasimov, G.N.; Gromov, V.F.; Ikim, M.I.; Ilegbusi, O.J.; Trakhtenberg, L.I. Effect of interaction between components of In<sub>2</sub>O<sub>3</sub>-CeO<sub>2</sub> and SnO<sub>2</sub>-CeO<sub>2</sub> nanocomposites on structure and sensing properties. *Sens. Actuators B* **2019**, *279*, 22–30. [[CrossRef](#)]
127. Yang, F.; Graciani, J.; Evans, J.; Liu, P.; Hrbek, J.; Sanz, J.F.; Rodriguez, J.A. CO oxidation on inverse CeO<sub>x</sub>/Cu(111) catalysts: High catalytic activity and ceria-promoted dissociation of O<sub>2</sub>. *Am. Chem. Soc.* **2011**, *133*, 3444–3451. [[CrossRef](#)]
128. Xu, L.; Song, H.; Dong, B. Preparation and bifunctional gas sensing properties of porous In<sub>2</sub>O<sub>3</sub>-CeO<sub>2</sub> binary oxide nanotubes. *Inorg. Chem.* **2010**, *49*, 10590–10597. [[CrossRef](#)]
129. Jiang, F.; Zhao, H.; Chen, H.; Xu, C.; Chen, J. Enhancement of photocatalytic decomposition of perfluorooctanoic acid on CeO<sub>2</sub>/In<sub>2</sub>O<sub>3</sub>. *RSC Adv.* **2016**, *6*, 72015–72021. [[CrossRef](#)]
130. Zappa, D.; Galstyan, V.; Kaur, N.; Munasinge, M.A.H.M.; Sisman, O.; Comini, E. Metal oxide-based heterostructures for gas sensors—A review. *Anal. Chim. Acta* **2018**, *1039*, 1–23. [[CrossRef](#)]
131. Kurmangaleev, K.S.; Bodneva, V.L.; Posvyansky, V.S.; Trakhtenberg, L.I. Sensory effect toward hydrogen in a nanostructured CeO<sub>2</sub>-In<sub>2</sub>O<sub>3</sub> system. *Russ. J. Phys. Chem. A* **2022**, *96*, 2056–2058. [[CrossRef](#)]
132. Wusiman, M.; Taghipour, F. Methods and mechanisms of gas sensor selectivity. *Crit. Rev. Solid State Mater. Sci.* **2022**, *47*, 416–435. [[CrossRef](#)]
133. Walker, J.; Karnati, P.; Akbar, S.A.; Morris, P.A. Selectivity mechanisms in resistive-type metal oxide heterostructural gas sensors. *Sens. Actuators B* **2022**, *355*, 131242. [[CrossRef](#)]
134. Mirzaei, A.; Leonardi, S.G.; Neri, G. Detection of hazardous volatile organic compounds (VOCs) by metal oxide nanostructures-based gas sensors: A review. *Ceram. Int.* **2016**, *42*, 15119–15141. [[CrossRef](#)]
135. Liang, Q.; Qu, X.; Bai, N.; Chen, H.; Zou, X.; Li, G.-D. Alkali metal-incorporated spinel oxide nanofibers enable high performance detection of formaldehyde at ppb level. *J. Hazard. Mater.* **2020**, *400*, 123301. [[CrossRef](#)]
136. San, X.; Li, M.; Liu, D.; Wang, G.; Shen, Y.; Meng, D.; Meng, F. A facile one-step hydrothermal synthesis of NiO/ZnO heterojunction microflowers for the enhanced formaldehyde sensing properties. *J. Alloys Compd.* **2018**, *739*, 260–269. [[CrossRef](#)]
137. Galstyan, V.; Ponzoni, A.; Kholmanov, I.; Natile, M.M.; Comini, E.; Sberveglier, G. Highly sensitive and selective detection of dimethylamine through Nb-doping of TiO<sub>2</sub> nanotubes for potential use in seafood quality control. *Sens. Actuators B* **2019**, *303*, 127217. [[CrossRef](#)]
138. Zhang, W.-H.; Zhang, W.-D. Fabrication of SnO<sub>2</sub>-ZnO nanocomposite sensor for selective sensing of trimethylamine and the freshness of fishes. *Sens. Actuators B* **2008**, *134*, 403–408. [[CrossRef](#)]
139. Hemmati, S.; Firooz, A.A.; Khodadadi, A.A.; Mortazavi, Y. Nanostructured SnO<sub>2</sub>-ZnO sensors: Highly sensitive and selective to ethanol. *Sens. Actuators B* **2011**, *160*, 1298–1303. [[CrossRef](#)]
140. Park, H.; Kim, J.-H.; Vivod, D.; Kim, S.; Mirzaei, A.; Zahn, D.; Park, C.; Kim, S.S.; Halik, M. Chemical- recognition-driven selectivity of SnO<sub>2</sub>-nanowire-based gas sensors. *Nano Today* **2021**, *40*, 101265–101266. [[CrossRef](#)]
141. Mirzaei, A.; Kim, J.-H.; Kim, H.W.; Kim, S.S. Resistive-based gas sensors for detection of benzene, toluene and xylene (BTX) gases: A review. *J. Mater. Chem. C* **2018**, *6*, 4342–4370. [[CrossRef](#)]
142. Pasti, I.A.; Gavrilov, N.M.; Mentus, S.V. Hydrogen adsorption on palladium and platinum overlayers: DFT study. *Hindawi Publ. Corp. Adv. Phys. Chem.* **2011**, *4–6*, 1–8. [[CrossRef](#)]
143. Molina, L.M.; Hammer, B. Active role of oxide support during CO oxidation at Au/MgO. *Phys. Rev. Lett.* **2003**, *90*, 206102. [[CrossRef](#)] [[PubMed](#)]
144. Yin, X.-T.; Wu, S.-S.; Dastan, D.; Nie, S.; Liu, Y.; Li, Z.-G.; Zhou, Y.-W.; Li, J.; Faik, A.; Shan, K.; et al. Sensing selectivity of SnO<sub>2</sub>-Mn<sub>3</sub>O<sub>4</sub> nanocomposite sensors for the detection of H<sub>2</sub> and CO gases. *Surf. Interfaces* **2021**, *25*, 101190. [[CrossRef](#)]
145. Nakate, U.T.; Ahmad, R.; Patil, P.; Wang, Y.; Bhat, K.S.; Mahmoudi, T.; Yu, Y.T.; Suh, E.-k.; Hahn, Y.-B. Improved selectivity and low concentration hydrogen gas sensor application of Pd sensitized heterojunction *n*-ZnO/*p*-NiO nanostructures. *J. Alloys Compd.* **2019**, *797*, 456–464. [[CrossRef](#)]

**Disclaimer/Publisher's Note:** The statements, opinions and data contained in all publications are solely those of the individual author(s) and contributor(s) and not of MDPI and/or the editor(s). MDPI and/or the editor(s) disclaim responsibility for any injury to people or property resulting from any ideas, methods, instructions or products referred to in the content.